UNIVERSITY OF DEBRECEN
FACULTY OF ENGINEERING
DEPARTMENT OF
MECHANICAL ENGINEERING

HIGH-FREQUENCY ACOUSTIC EMISSION MEASUREMENT IN CHARPY IMPACT TESTING COMBINED WITH BARKHAUSEN NOISE ANALYSIS AND RESIDUAL STRESS LEVEL MEASUREMENT.

THESIS

Orynbassar Beibarys

Operation and Maintenance Specialization

Debrecen

2025

Table of Contents

List of Abbreviations

1. **AE:** Acoustic Emission
2. **BHN:** Barkhausen Noise
3. **CTOD:** Crack Tip Opening Displacement
4. **DAQ:** Data Acquisition
5. **FFT:** Fast Fourier Transform
6. **HDM:** Hole Drilling Method
7. **HV:** Vickers Hardness
8. **IEPE:** Integrated Electronics Piezo-Electric
9. **MARSE:** Measured Area under the Rectified Signal Envelope
10. **ND:** Neutron Diffraction
11. **NDT:** Non-Destructive Testing
12. **RMS:** Root Mean Square
13. **RUL:** Remaining Useful Life
14. **UT:** Ultrasonic Transducer
15. **VI:** Virtual Instrument
16. **XRD:** X-ray diffraction

Table of Notations

Acoustic Emission Parameters:

$R\ [s^{-1}]$	AE event rate
$N\ [-]$	Number of AE events
$\Delta t\ [s]$	Monitoring time interval
$X(f)\ [-]$	Frequency-domain representation of the AE signal
$x(t)\ [V]$	Time-domain waveform
$f\ [Hz]$	Frequency
$j\ [-]$	Imaginary unit

Barkhausen Noise Parameters:

$J\ [-]$	Magnetization
$B\ [-]$	Flux density
$RMS\ [V]$	Root Mean Square
$x_i\ [V]$	Amplitude of the BHN signal at time point i
$n\ [-]$	Total number of data points

Entropy Parameters:

$H\ [Bits]$	Shannon Entropy
$H\ [A/m]$	Magnetic field intensity
$x\ [-]$	Distinct discrete state or amplitude bin
$p(x)\ [-]$	Probability of the acoustic signal occupying state x

List of Formulas

$R = \frac{N}{\Delta t}$	AE event rate
$X(f) = \int_{-\infty}^{\infty} x(t) \cdot e^{-j2\pi f t}\, dt$	Fourier Transform
$RMS = \sqrt{\frac{1}{n}\sum_{i=1}^{n} x_i^2}$	Root Mean Square (RMS)
$H = -\sum p(x) \log p(x)$	Shannon's entropy

1 Introduction

Internal residual stresses influence the behavior of structures. They limit their performance, fatigue, and fracture resistance. These stresses often occur after welding, machining, plastic deformation, or heat treatment. Compressive residual stress can be beneficial as they can increase material lifetime, on the other hand tensile residual stress can be dangerous, and they can cause sudden failure even under service conditions. It is crucial to accurately interpret these stresses is critical for ensuring structural integrity and extending the life of components.

This research proposes the integration of two non-destructive testing (NDT) techniques **High-Frequency Acoustic Emission (AE)** and **Barkhausen Noise (BHN) Analysis.** The purpose of combining these approaches is to avoid conventional internal stress evaluation methods, because they are costly, require a long time, or invasive. The unified diagnostic system that can detect, monitor, and evaluate residual stress states in ferromagnetic materials.

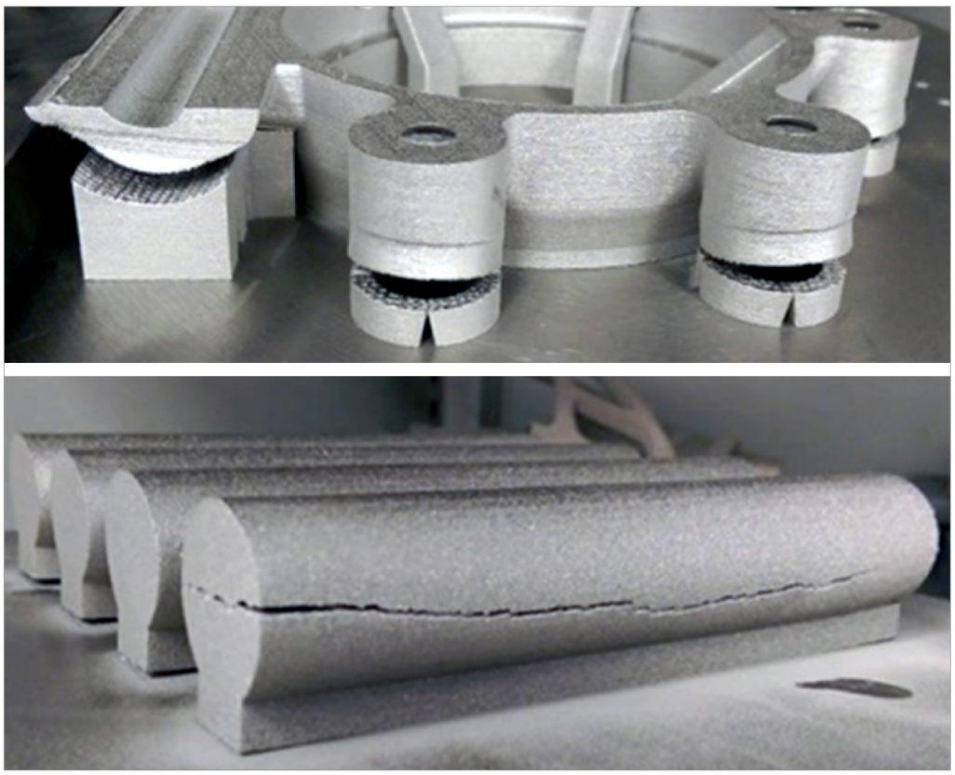

Figure 1.1 Residual Stress Consequences [1]

- **Research Motivation and Problem Statement**

Acoustic emission analysis and Barkhausen noise analysis, separately, are valuable NDT methods for material evaluation. However, these two methods were not yet integrated to detect residual stress. AE is applied in monitoring during mechanical testing; capturing elastic waves generated by micro cracking and sudden energy releases. Magnetic noise caused by domain wall movements under alternating magnetic field makes up BHN analysis. Magnetic jumps are then used to evaluate stress levels inside the material.

Guo et al in 2022 introduced several techniques to interpret the stress distribution state more efficiently, as correct stress state understanding is essential in safety-critical applications [2].

Recent studies demonstrate the feasibility of using multidirectional BHN for stress analysis techniques with high sensitivity and adaptability [3].

This thesis focuses on the need for improved residual stress assessment methods by introducing an integration of high-frequency Acoustic Emission and Barkhausen Noise techniques during Charpy impact testing. The four tasks will support the development of an integrated approach.

- Design an experimental setup for AE measurement in Charpy impact tests.
- Analyze AE signal characteristics to correlate with material deformation, fracture, and BHN signals.
- Develop a method for evaluating residual stress levels based on AE and BHN analysis.
- Compare the experimental results with existing material stress analysis methods.

2 Literature review

2.1 Introduction to Residual Stresses

Residual stresses are the stresses in the material which can appear without the applied load. Moreover, they affect the characteristics of the components detrimentally. This can lead to the failure of structural integrity. Residual stress can also impact fatigue strength and resistance to fracture. Residual tensile stresses tend to increase crack growth, which shortens the lifetime of a component. It is crucial to quantify the internal stresses, because those stresses can affect the maximal strength of the mechanical component According to SinTechnology Ltd. residual stresses can be caused by the following main factors [4]:

- Uneven temperature distribution during casting welding, molding, or heat treatment
- Material removal or deformation methods like turning and forging.
- Thermal surface treatments like tempering, welding, or grinding.
- Surface modification techniques such as sandblasting and shot peening.

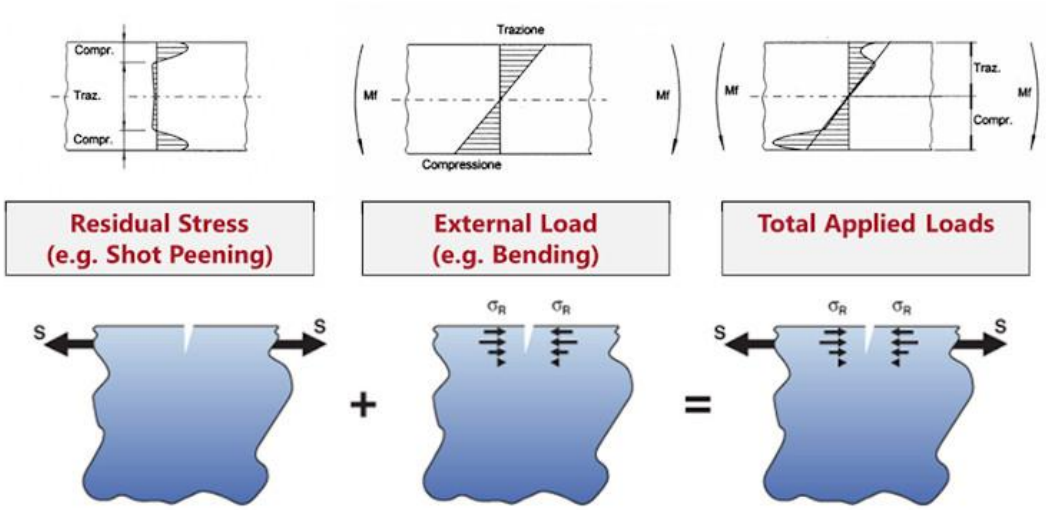

Figure 2.1 Residual Stress effect [4]

2.2 Conventional Methods for Residual Stress Measurement

Evaluation of the residual stresses amount is essential, because knowing that the behavior of the material under service conditions can be foreseen. There are three

main methods currently utilized to access the internal stress: X-ray diffraction method, neutron diffraction, and the hole-drilling method.

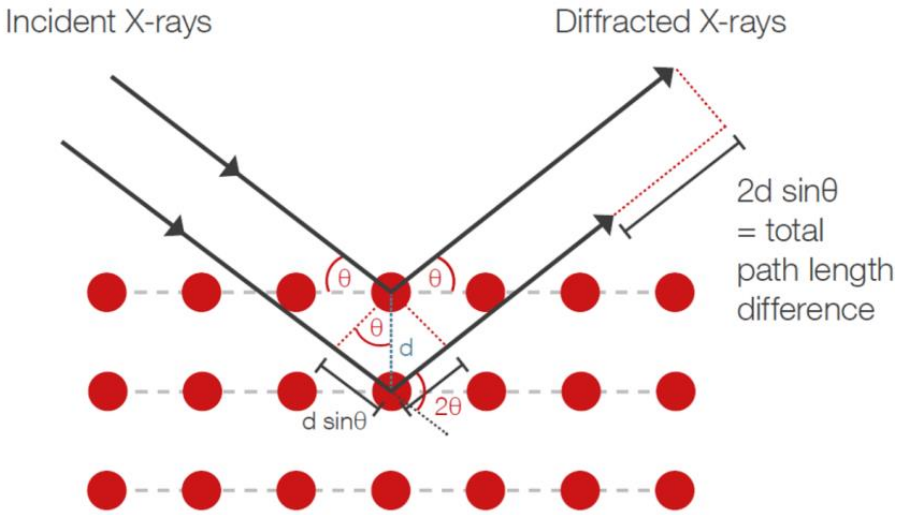

Figure 2.2 X-ray diffraction method [5]

1. X-ray diffraction. This approach is used only on crystalline materials. The residual stresses cause elastic strains which lead to shift in diffraction angles. Afterwards, by knowing elastic parameters, the angle shifts measured, to determine residual stresses [6].

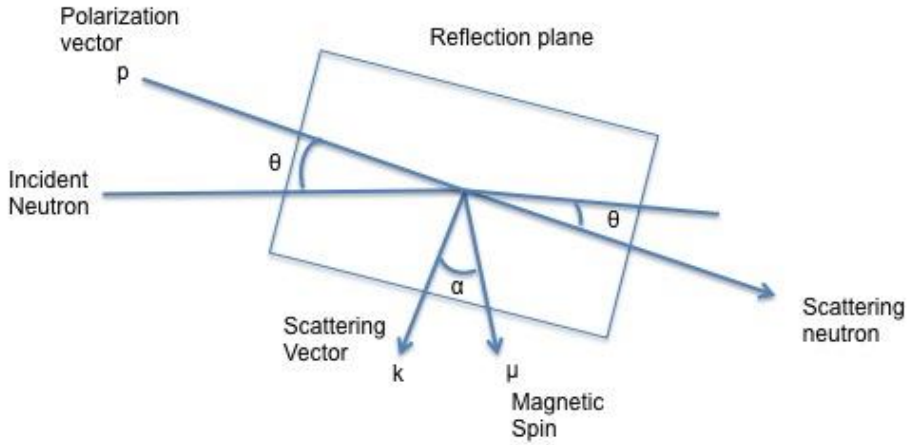

Figure 2.3 Neutron diffraction method [7]

2. Neutron diffraction method (ND) provides residual stress tensor analysis on thick components [6]. ND measures the elastic strain by calculating stress with Hooke's law. Expensive equipment makes this method unsuitable for scalable and industrial applications.

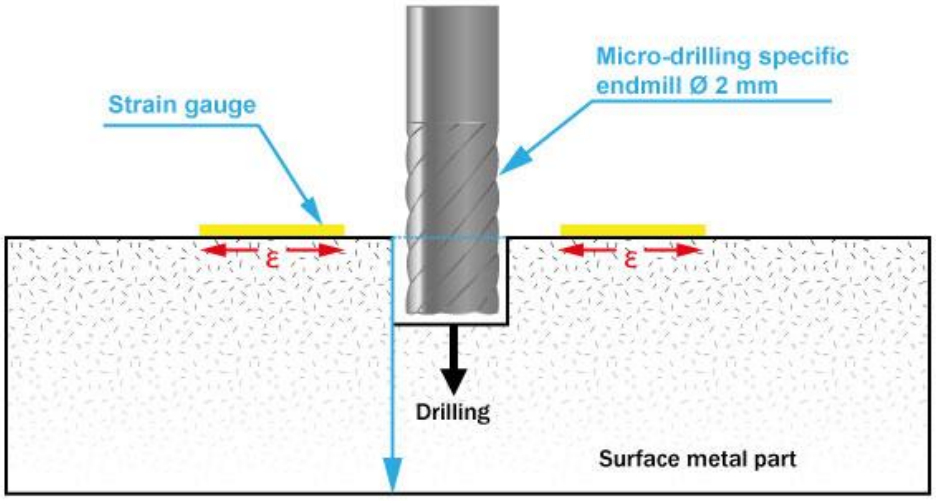

Figure 2.4 Hole drilling method [8]

3. Hole drilling method (HDM). A small hole is drilled from material surface, then the strain relief is recorded by strain gauges. The destructive nature of this approach makes its application unreliable as different specimens and parts can have varying number of internal stresses.

While these methods are well-established, they often require access to the material surface and can be time-consuming and costly. Additionally, some methods may not be suitable for complex geometries or materials with heterogeneous microstructures.

2.3 Charpy Impact testing

This method is much easier and less expensive to conduct and is evaluated by K_{Ic}CTOD (Crack Tip Opening Displacement) [9]. The setup of the machine includes specimen holds, a pendulum which transfers the hit energy, and the notched specimen. The notch helps control where the crack starts. After the impact, the machine tells how much energy was used to break the specimen [10].

Figure 2.5 Charpy Impact test machine

The toughness of the material directly correlates with the temperature [11]. For this research, Charpy testing is not used for calculating material toughness, but to create the right fracture conditions for Acoustic Emission (AE) monitoring. When the notched specimen undergoes sudden impact and the fracture initiation starts, AE sensors can detect signals from the fracture. These signals can be utilized to detect crack development phases.

Figure 2.6 Acoustic emission sensor [12]

During the impact testing Barkhausen Noise (BHN) signal is continuously measuring the magnetic jumps in the material, which depicts the internal stress state.

2.4 Acoustic Emission (AE)

AE signals are elastic waves which are released due to the deformation inside the material's microstructure. These energy releases are linked with the fracture of initiation and propagation [13]. Real-time data gathered from AE analysis during material loading can be used to foresee fracture development. Amplitude, counts, energy, rise time, duration, event rate, and other signal parameters can be analyzed.

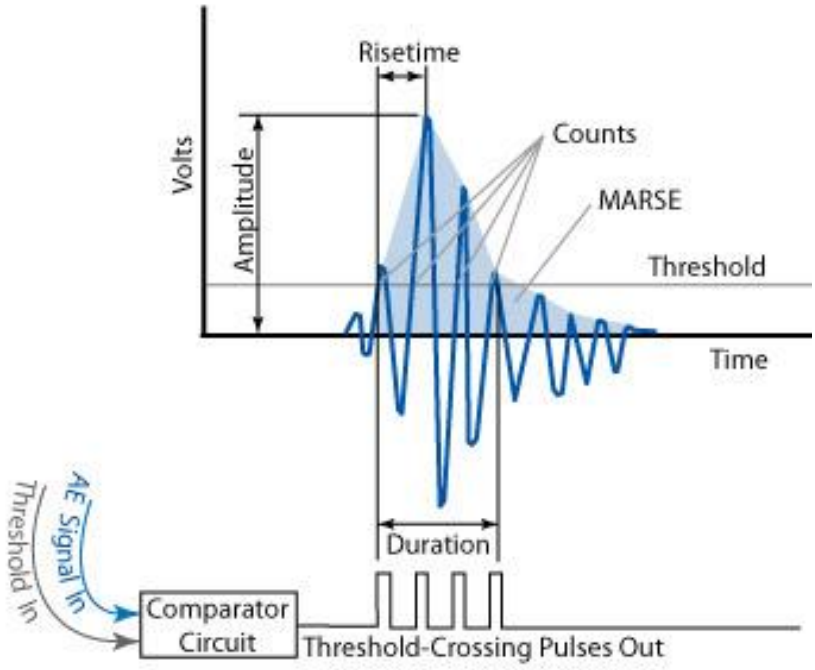

Figure 2.7 Components of Acoustic signal [14]

The AE event rate, for instance, is defined as:

$$R = \frac{N}{\Delta t} \qquad (1)$$

Where:

- R is the AE event rate (events per second),
- N is AE events number,
- Δt is the monitoring time interval.

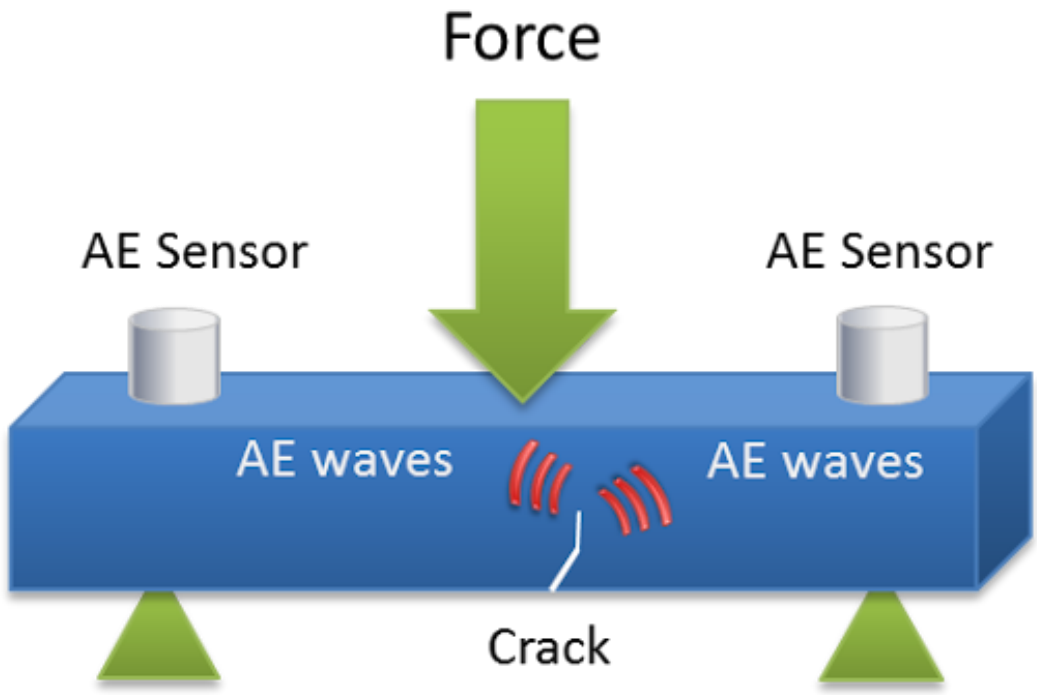

Figure 2.8 Acoustic Emission measurement [15]

Higher AE activity correlates with increased microstructural damage, indicating crack nucleation or propagation. These AE parameters deepen the understanding of the mechanical behavior of a material under a dynamic impact. Furthermore, according to A. Carpinteri fracture mode and Remaining Useful Life can be accessed [16]. Fast Fourier Transform (FFT) frequency domain analysis helps to differentiate between crack initiation, plastic deformation, and material failure:

$$X(f) = \int_{-\infty}^{\infty} x(t) \cdot e^{-j2\pi ft}\, dt \qquad (2)$$

Where:

- X(f) is the frequency-domain waveform,
- x(t) is the time-domain waveform,
- f is the frequency,
- j is the imaginary unit.

AE has been successfully applied in both laboratories and practical conditions to monitor damage in structures. AE can help detect stress relaxation or crack formation related to internal stress redistribution. AE complements other diagnostic techniques such as Barkhausen Noise (BHN) analysis and X-ray diffraction.

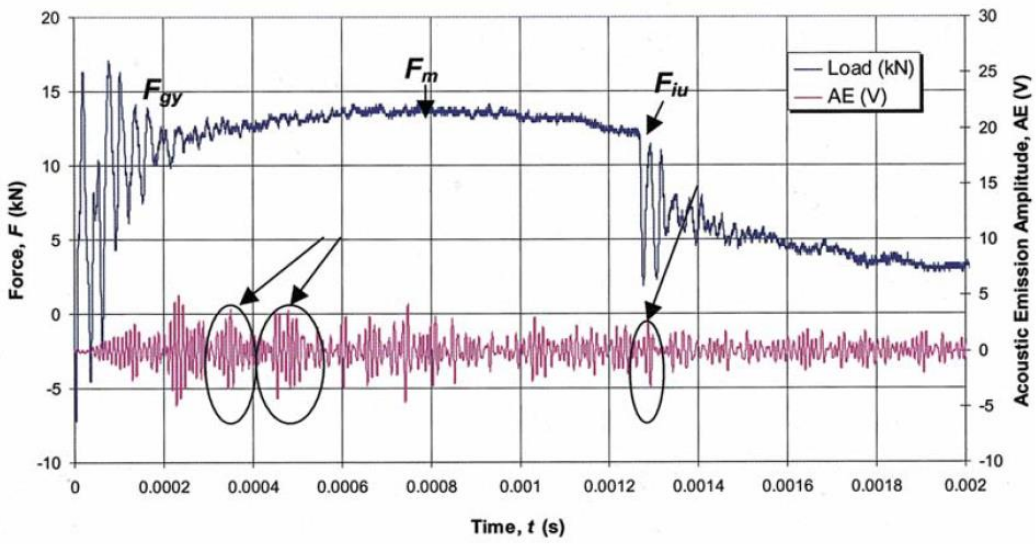

Figure 2.9 Force and acoustic emission curves [17]

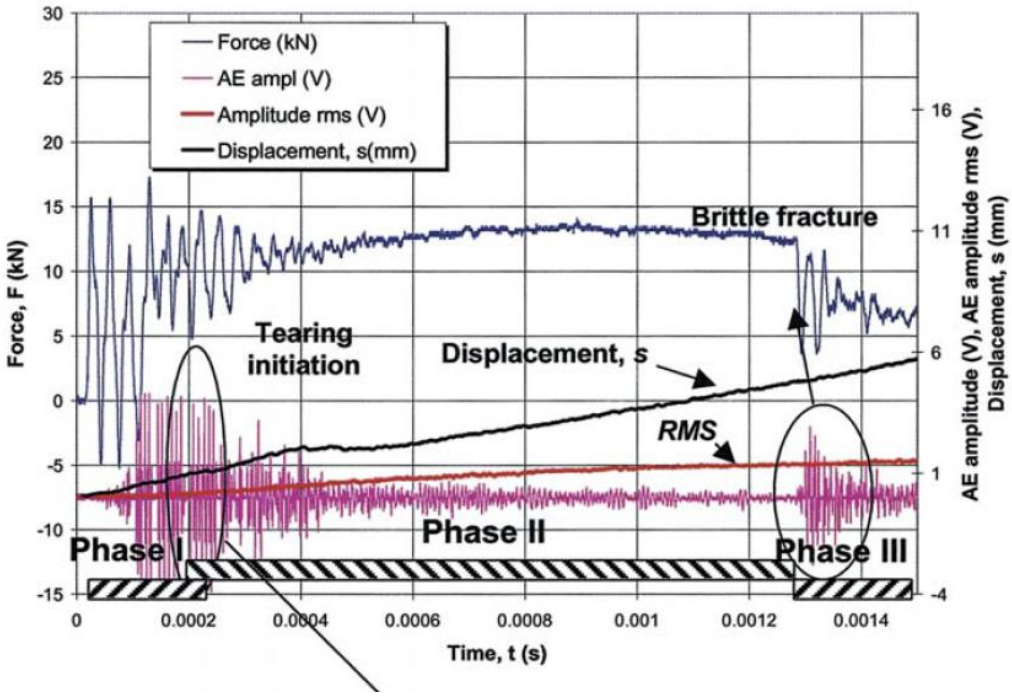

Figure 2.10 Force, acoustic emission, and displacement curves [17]

Research of Tronskar et al. proved that AE demonstrates high sensitivity in detecting initial stages of ductile tearing [17]. Three fracture phases were identified based on AE signal characteristics: Phase I (mechanical oscillations and yielding), Phase II (onset of ductile crack initiation), and Phase III (final brittle fracture) as it was shown in figures 2.9 and 2.10

During the initial stages of material loading, the AE activity is minimal, only the waves from machine vibration can be detected by the sensors [18]. An increase of

AE event counts usually characterizes the approaching to the yield point. The beginning of plastic deformation corresponds to an increase in AE activity. High bursts of AE amplitude come from sudden release of stored energy and signalizing crack initiation processes. Previous research demonstrated that these peaks correlate with onset of ductile tearing. By analyzing AE signals, fracture initiation can be detected and classified.

The measurement setup designed by Tronskar et al is like the planned research setup as it does not require complex technology to attach to the Charpy Impact tester. The signals were recorded using a basic amplifier and high-speed oscilloscope. In a current study, a similar setup will be adopted, allowing AE to be applied in parallel with Barkhausen Noise measurements for residual stress analysis.

2.5 Barkhausen Noise (BHN)

Barkhausen Noise (BHN) analysis is an NDT method used to detect changes in internal stress state of ferromagnetic structures. It relies on the detection of sudden jumps of magnetic domain walls when the material is exposed to an alternating magnetic field.

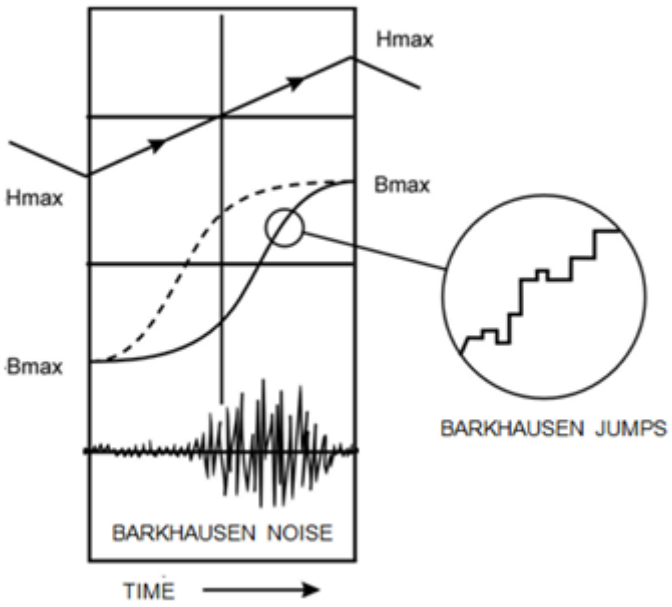

Figure 2.11 Barkhausen effect [19]

Where:

- J – Magnetization
- B – Flux density
- H – Function of magnetic field intensity

The presence of residual stress influences the energy barriers for domain wall motion, thereby affecting the intensity and pattern of the BHN signal. Tensile stresses increase the amplitude of domain movement, while compressive stresses decrease the BHN signal amplitude. This stress sensitivity makes BHN signal analysis suitable for non-destructive measuring of residual stress levels.

[20] In 2018 research by Aki Sorsa demonstrated that BHN signals can be used to identify the residual stress. Their objective was to evaluate the interaction between variable shot peening and their BHN signatures.

The measurement principle of the Barkhausen noise is the following:

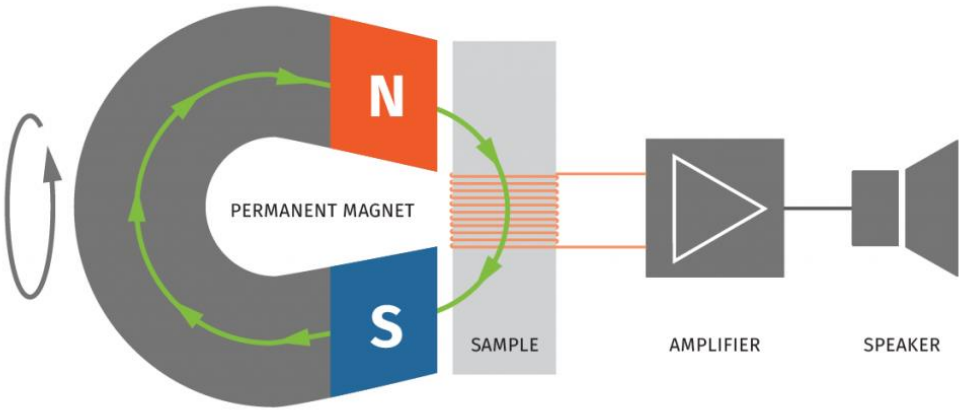

Figure 2.12 Barkhausen noise measurement setup [21]

2.5.1 Root Mean Square (RMS) in BHN

The Root Mean Square value of the BHN signal intensity measures the energy of the signal. It also can be used to evaluate residual stress levels on magnetic response of the specimen.

$$RMS = \sqrt{\frac{1}{n}\sum_{i=1}^{n} x_i^2} \qquad (3)$$

Where:

- x_i - amplitude of the BHN signal at time point i
- n - number of data points

In 2017, Binayaka Nahak described that BHN signal parameters are sensitive to changes in structure and hardness [22].

2.5.2 BHN in residual stress level measuring

Barkhausen noise analysis is efficient in evaluating the material's stress state [23]. This NDT method does not provide stress value, but it gives the foundation to evaluate stress state change. It is possible to accomplish this successfully and without causing any damage by using a calibration procedure. Barkhausen noise is also used in the assessment of welding stresses.

2.5.3 Integration of AE and BHN for Stress Evaluation

The combination of Barkhausen Noise (BHN) and Acoustic Emission (AE) techniques offers a powerful hybrid approach to residual stress analysis and fracture evaluation in ferromagnetic materials. BHN provides the method to mark the near-surface stress state after the deformation, while AE detects the signals during the crack initiation and propagation processes defining distinct phases of deformation. By integrating both approaches, the structural integrity of the specimen can be evaluated in a more sophisticated manner.

The benefits of using AE and BHN together were highlighted in studies involving dynamic loading or surface modification processes. For example, AE was used to detect the beginning of ductile tearing, while BHN testing measured change of the stress state of the specimen. AE allows for fracture phase differentiation (crack initiation, and final rupture), on the other hand BHN can be used to grade stress distribution induced by those fractures.

Non-destructive nature and simple setup make AE and BHN research compatible. AE sensors can be attached during testing without affecting specimen behavior, and BHN measurements can be conducted after the load. Additionally, since both techniques generate digital signals that can be processed with analytical tools, they make synchronized analysis or correlation models possible. In this thesis, the AE technique will be applied during instrumented Charpy impact testing to capture crack initiation and fracture energy events, while BHN measurements will be conducted before and after the test to assess the pre-existing and post-impact stress distribution on same specimen region.

3 Design of the experimental setup

3.1 Specimen Preparation and Characterization

For a systematic investigation into the influence of various microstructures on Acoustic Emission (AE) and Barkhausen Noise (BHN) signals, a controlled heat treatment was adopted. In total, 27 samples were prepared and divided into three different experimental groups, with nine samples in each group.

To analyze the effects of microstructural changes on AE and BHN signatures, a heat treatment was done. The 27 samples were subjected to an initial heating cycle to 900°C. This temperature was deliberately chosen since it represents the austenitization temperature of the steel. Upon heating carbon steel above its upper critical point (above the A3 line in the Fe-C phase diagram), the BCC crystal structure at room temperature converts entirely to an FCC structure referred to as austenite. The two key roles of the austenitization cycle include dissolving carbon in a solid solution and relieving any residual manufacturing stresses in the material. Through the austenitization step, all 27 samples were standardized in terms of their microstructure before being divided into the cooling batches.

The mechanical properties, residual stress states, and fracture behaviors of the specimens depend solely on the rate at which the austenite cools down. The furnace cooling, air cooling, and water quenching used for this experiment have been selected to ensure that the entire range of phase transformations exhibited by the material is covered.

Group 1: Slow cooling in the furnace.

Group 2: Air cooling (normalizing).

Group 3: Rapid cooling in water (quenching).

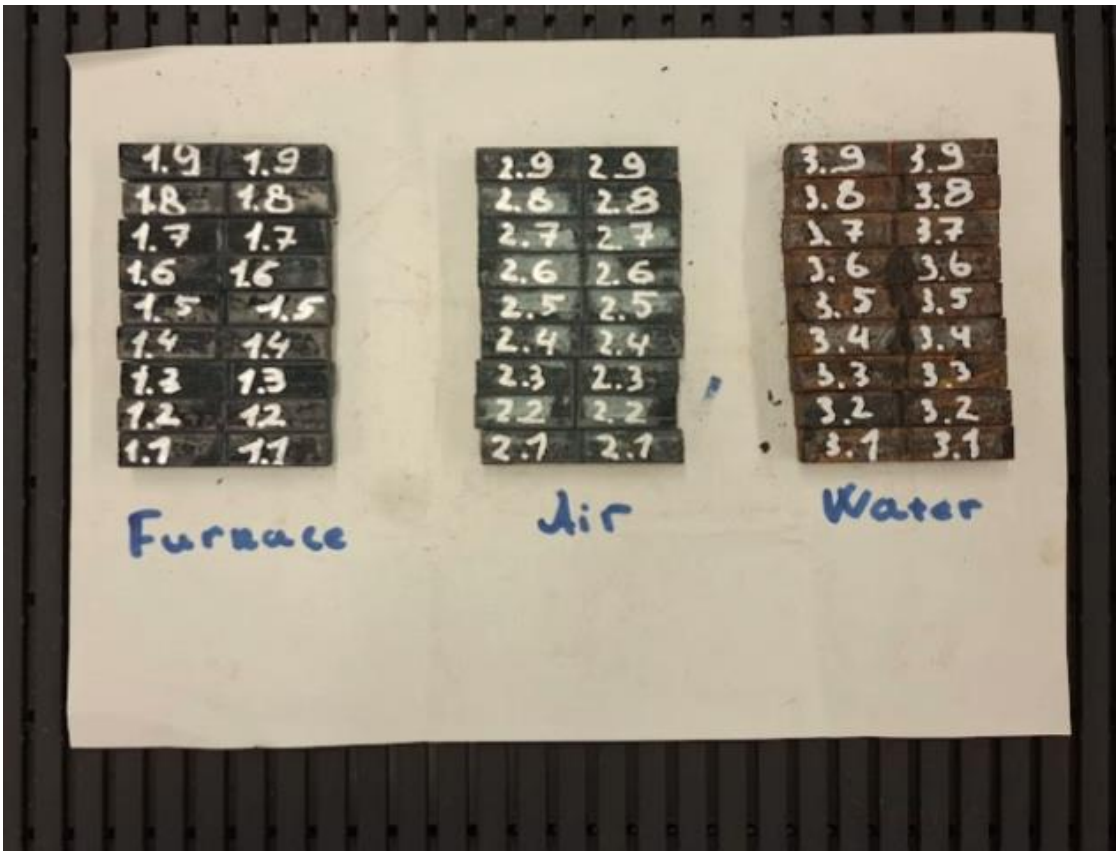

Figure 3.1 Specimen divided into groups: Furnace-, Air-, Water-cooled

After the heat treatment, the surface hardness was measured for all the samples to provide a mechanical base. Hardness measurements were carried out for all the samples using an ultrasonic Vickers hardness tester.

Figure 3.2 Ultrasonic Hardness measurement device

Note: The unusually low hardness measured on the samples quenched in water (about 143 HV) is an indication of significant decarburization of their surface during the furnace heating stage at 900°C. Taking into account the fact that the ultrasonic hardness tester measures the hardness only of the sample's surface layer, we can assume that its carbon content is low due to the formation of the ferritic structure.

The mean hardness results for the different cooling schemes are tabulated below:

Table 3.1 Hardness Values (HV)

Measurement Number	Furnace	Air Cooled	Water Cooled
1	287.55	373.21	134
2	326.07	332.61	145
3	325.36	350.53	142
4	186.69	344.85	137
5	228.67	422.25	140
6	328	380.57	151
7	291.24	368.29	135
8	297.58	357.31	153
9	288.57	336.43	169

3.1.1 Charpy Impact Testing Equipment and Procedure

In this study, the test was conducted using a pendulum-type Charpy impact testing machine (Wance Pendulum Impact Testing Machine) capable of delivering energy of 450 J.

Figure 3.3 Wance Charpy Impact Testing Machine

The specimens were prepared according to the standard, with a rectangular cross-section of [60 mm × 10 mm × 10 mm] and a V-notch of [2 mm depth with a 45° angle].

The 3D view of the Charpy Impact test specimen is shown below:

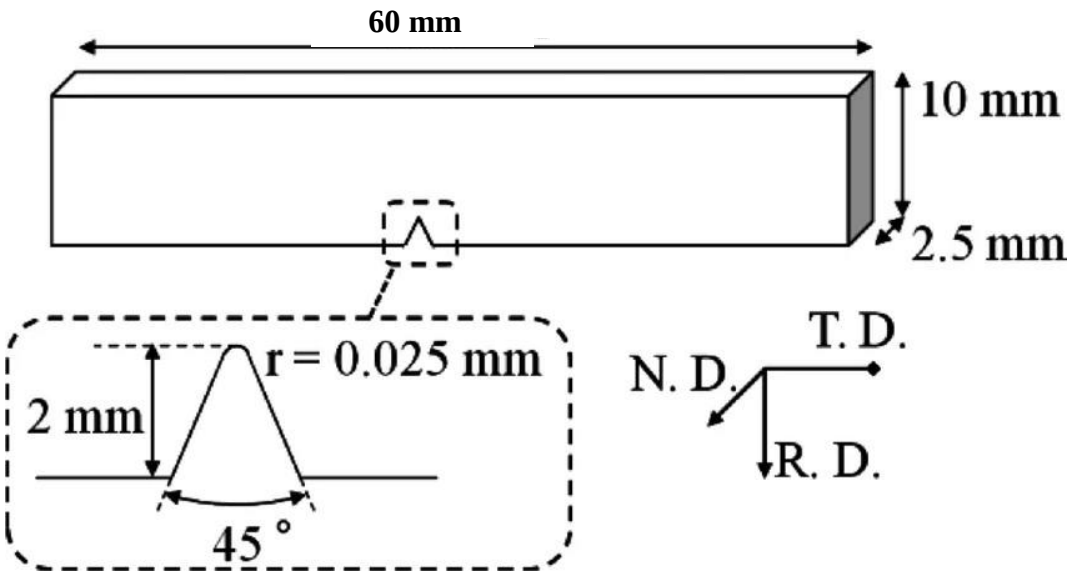

Figure 3.4 Specimen Dimensions [24]

Figure 3.5 Specimen after impact test

The head of the machine is made of hardened steel to withstand the operation period of the testing machine. It is connected to the high-mass pendulum made to transmit 450 Joules of energy.

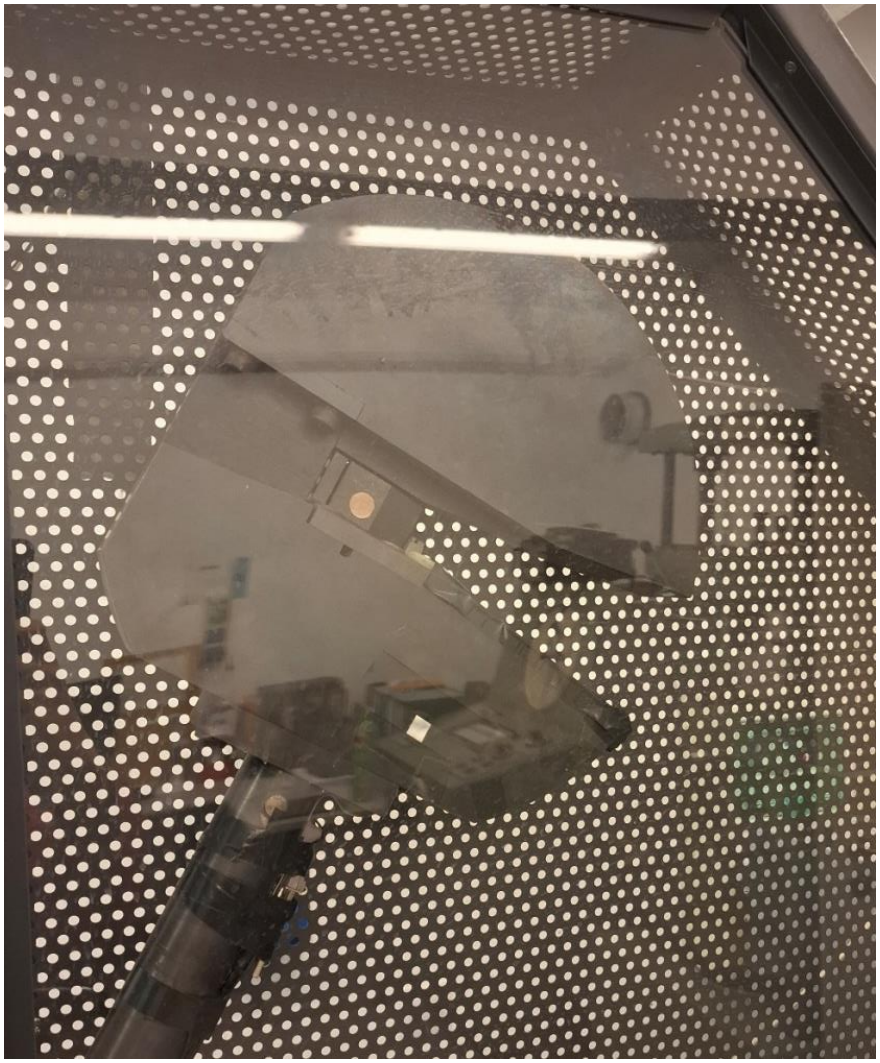

Figure 3.6 Charpy Impact testing machine head

The Charpy Impact testing method is suitable for this research for several reasons:

1. Tests provide a controllable and repeatable way of sudden dynamic fracture.
2. High-strain rate fracture generates high-energy fracture events in a brief time, which produce strong AE bursts that are distinguishable.
3. Precise timing of impact allows to easily synchronize the trigger events.
4. The standardized specimen geometry reduces the variation of AE signal patterns.
5. Various stages of crack propagation can be captured by ultrasonic sensors.

3.1.2 Measurement setup

The measurement setup of the AE signal processing system is not complicated; the main idea was acquired from the research described in the literature review section.

Key components include:

1. Wance 450 J Charpy Impact Testing machine
2. Ultrasonic Transducer
3. Pulse generator Type TR-0331
4. NI 9234 – 4-Channel, 24-Bit IEPE Sound and Vibration Input Module
5. Coaxial cable with BNC type connection

Ultrasonic Transducer (UT) utilized in this research can emit/transmit acoustic sound of up to 1 MHz the wide bandwidth allows to gather acoustic waves at different frequency levels, consequently those signals can be used in Fast Fourier transform analysis. Furthermore, it was observed that the acoustic emission of fracture propagation usually occurs at frequencies between 100 KHz – 1 MHz

Figure 3.7 Ultrasonic Transducer

Pulse Generator has variable parameters like frequency, delay, and width of the signal. The analogue device will output the base signal, which could be the lower limit of integration. Ultrasonic transducer outputs generated signal into the frame of the Impact testing machine.

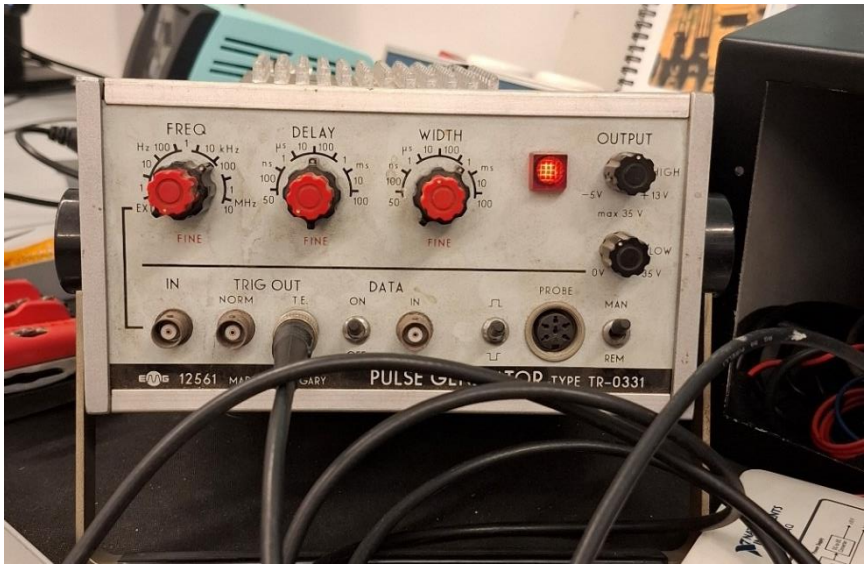

Figure 3.8 Pulse Generator

The connection of the pulse generator output and frame looks like the following:

Figure 3.8 Connection of Base signal to Machine

3.1.3 Acoustic Receiving and Transmitting Units

The primary acoustic emission sensor was placed to detect the micro-fracture-induced acoustic signals. This sensor was fixed to the front panel of the testing machine. To ensure the highest degree of structural rigidity for the machine and the sensor, a specially designed steel frame was welded to the wall of the machine.

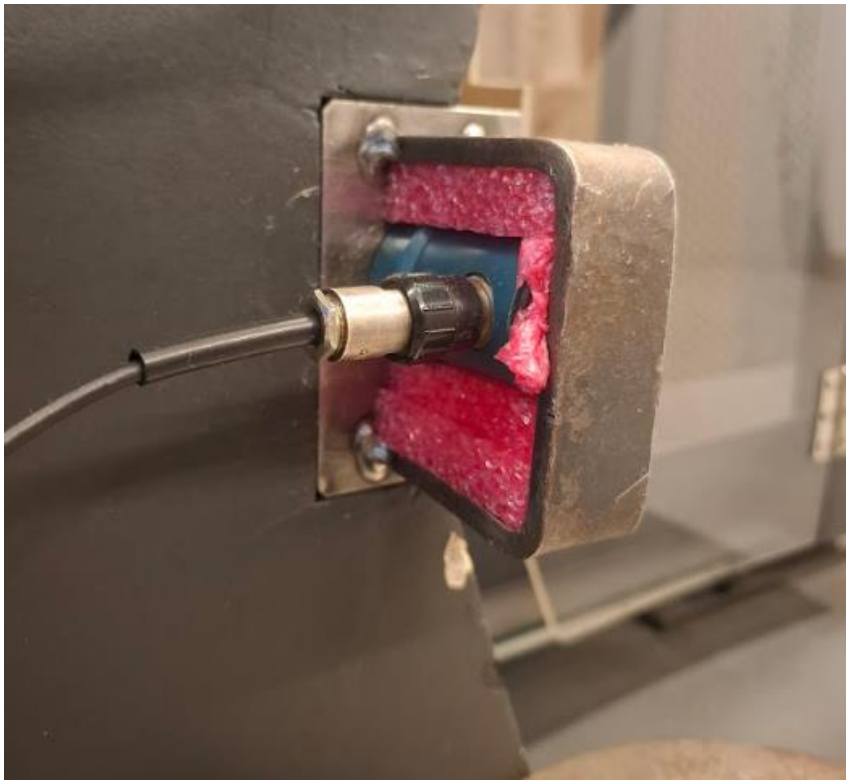

Figure 3.9 AE sensor connection

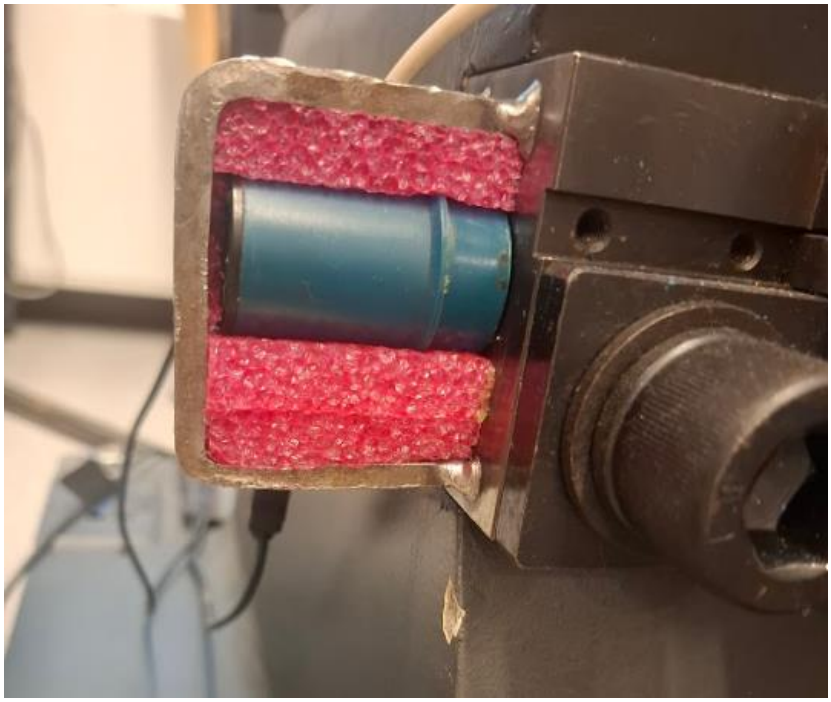

Figure 3.10 AE sensor connection

The design of the welded steel frame was critical for several reasons:

- Proximity: The welded steel frame was designed to minimize the distance between the source of the acoustic emission (the V-notch in the specimen) and the measurement device. Minimizing this transmission path was essential to successfully gather the weakest bursts of acoustic emission before they attenuated within the massive steel body of the impact tester.
- Acoustic transmission: The welded steel frame was designed to minimize the impedance mismatch between the source and the detector. This allowed the high-frequency acoustic signals (100 kHz to 1 MHz) generated due to crack propagation to travel directly from the anvil to the sensor without any attenuation caused by a bolted joints or soft coupling materials

To provide the system with the constant reference signal for further integration, the secondary transmitting unit was utilized. For this unit, the housing was created using 3D printing technology. The housing was created using polymer, thereby ensuring that the unit was securely attached and aligned.

3.1.4 Signal Amplification

Barkhausen Noise (BHN) measurement is based on the detection of extremely small levels of electromotive force that result from the magnetic domain wall movements. However, it is important to note that the low levels of the magnetic response signal require signal conditioning as an essential prerequisite before the signal is digitized.

As a way of reducing the attenuation of the data and improving the signal-to-noise ratio significantly, hardware amplifiers were integrated into the system. This was achieved by connecting the amplifiers in series between the BHN sensor and the associated data acquisition (DAQ) module. This ensured that the weak magnetic response signal was amplified before being processed in the LabVIEW environment.

3.2 Data Acquisition System and Software Architecture

To synchronous and high-resolution data acquisition from various sensors, the signal acquisition architecture has been implemented in the LabVIEW environment. The handling of a large volume of high-frequency data generated during the millisecond-scale fracture event requires efficient hardware interfacing to avoid any bottlenecks in the data acquisition or the sampling rate.

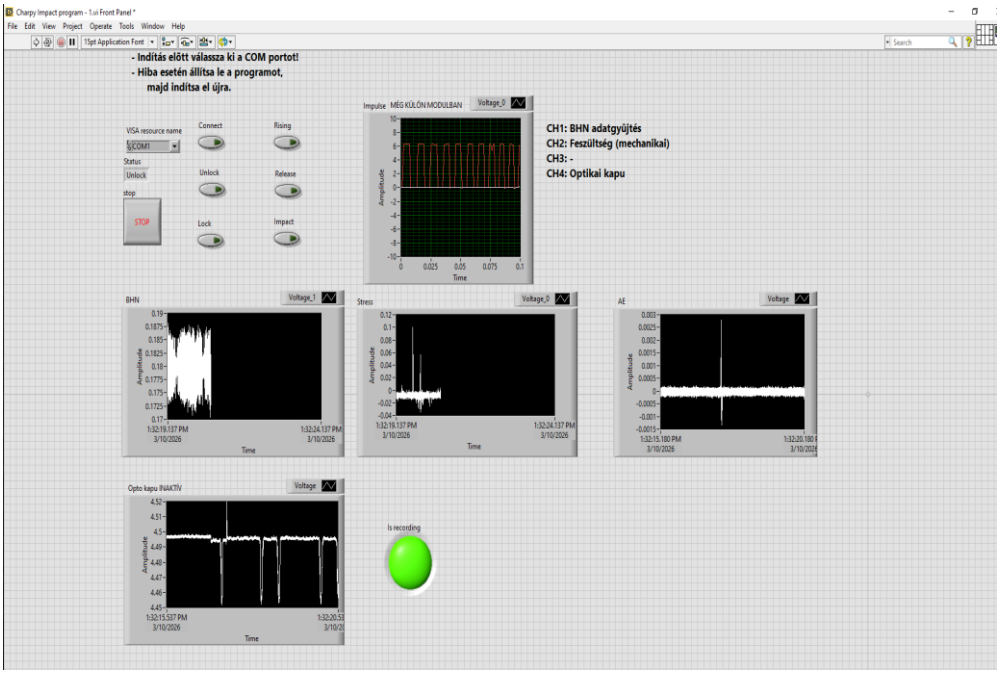

Figure 3.11 LabVIEW Front Panel

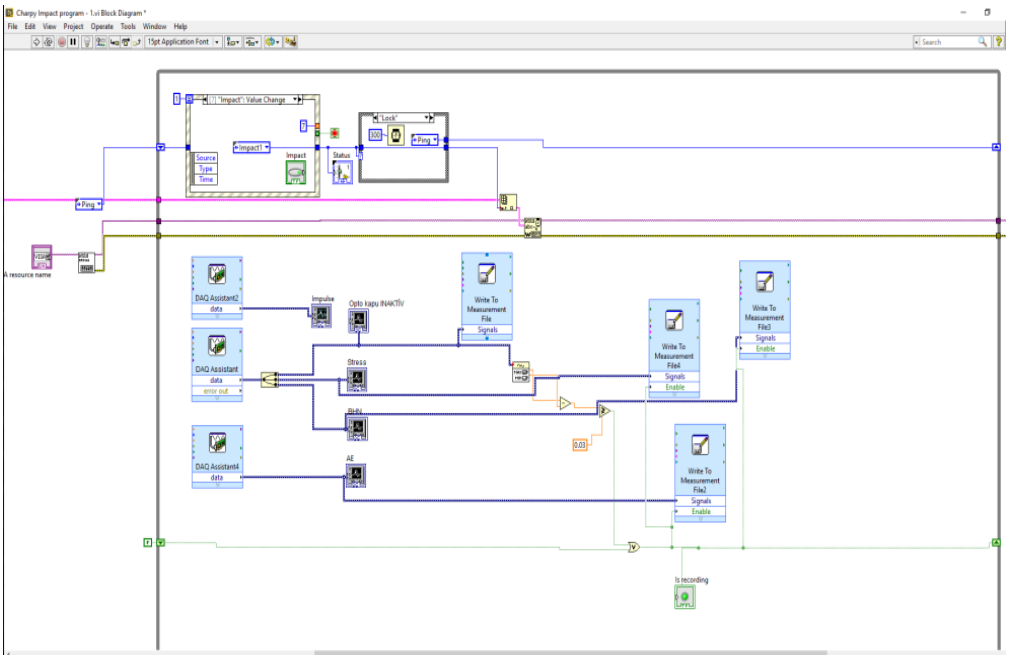

Figure 3.12 LabVIEW Back Panel

3.2.1 DAQ Hardware Configuration

To optimize the parallelization of the data acquisition process, the data acquisition load was distributed among three independent Data Acquisition (DAQ) units. The channel allocation was as follows:

DAQ Unit 1 (Acoustic Acquisition): This unit is dedicated to acquiring the high-frequency signals of Acoustic Emission (AE). The isolation of this channel is essential to maintain the highest sampling rate necessary to preserve the integrity of micro-fracture acoustic waves.

DAQ Unit 2 (Combined Modules): A multiplexed unit designed to simultaneously acquire Barkhausen Noise (BHN), mechanical stress gauge, and optical gate signals.

DAQ Unit 3 (Impulse Tracking): Specifically allocated to track the impulse signal emitted during the pendulum strike to obtain an exact time mapping of energy transfer.

3.2.2 Automated Triggering Logic

Given the highly transient nature of the Charpy impact test, manual initiation of data logging is impossible. Consequently, an automated, hardware-in-the-loop triggering protocol was engineered using the optical gate positioned along the pendulum trajectory.

Within the LabVIEW Virtual Instrument (VI), the continuous voltage output from the optical gate was actively monitored. The software was programmed to evaluate this signal to detect a sudden voltage spike, which indicates the pendulum entering the immediate strike zone. The activation threshold was strictly defined as a voltage jump of **0.03 V**.

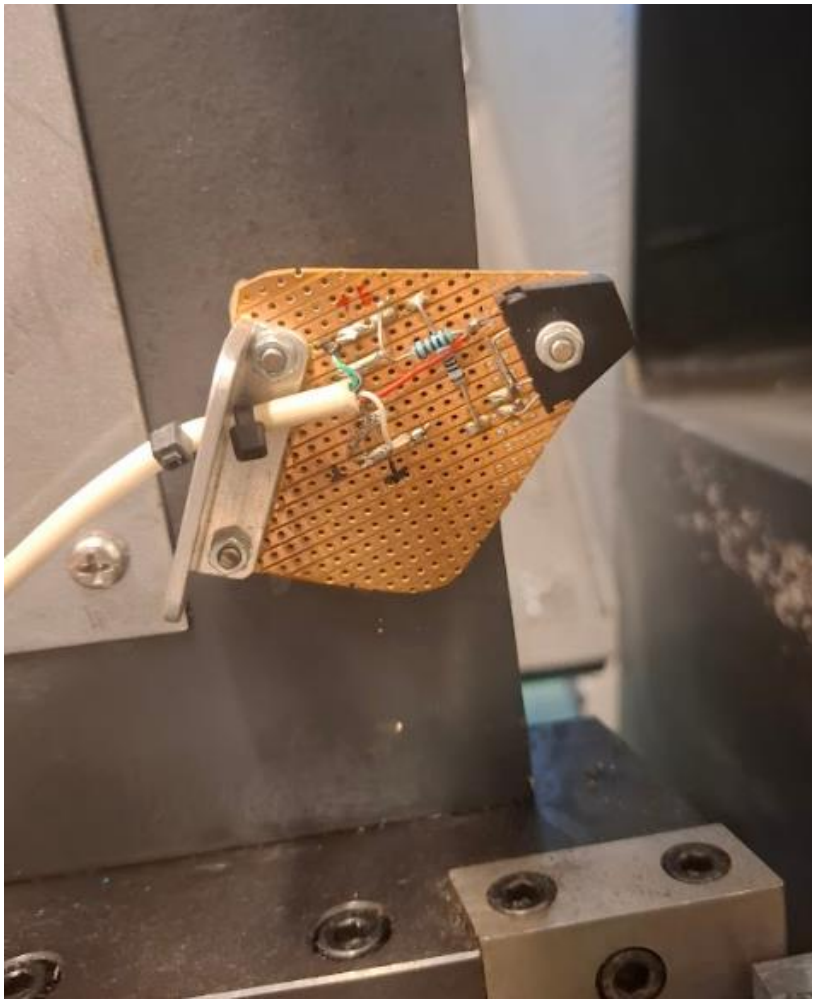

Figure 3.13 Optical gate

To identify the True and False state of the optical gate, the pendulum was placed in front of the sensor. As the pendulum appeared in front of the sensor, the voltage value which is not steady dropped usually from 4.51 to 4.48-4.47, in other cases it could drop from 4.46 to 4.42. Because of this factor analyzing the difference value of the voltage in optical gate was to be set.

When the optical gate signal difference exceeds this **0.03 V** threshold, a comparator function within the LabVIEW block diagram outputs a Boolean "True" state. This Boolean signal is wired directly to the selector terminal of a designated Write to Measurement file structure. The execution of this "True" case instantaneously initiates the synchronized data recording sequence across all three active DAQ units.

3.2.3 Data Streaming and Storage

As soon as the Case Structure is triggered by the impact of the pendulum, the multi-channel data streams from the data acquisition units are directly written to the disk. For the efficient handling of the high-volume and high-frequency data

without any buffering errors, the LabVIEW system has been configured for the output of the data in the Technical Data Management Streaming File (.tdms) format.

The ability of the. tdms format to capture exact timestamps and high disc recording speeds made it an efficient solution for the research purpose. This format saves metadata of all four channels and is convenient for further data processing using Python libraries.

3.2.4 Impact Testing Execution and Data Acquisition Sequence

After the configuration of the LabVIEW setup, sensor calibration, and integration of the signal amplifier, the physical testing phase was initiated. The experimental protocol was conducted in a systematic manner across all 27 heat-treated specimens, including those that were furnace-cooled, air-cooled, and water-quenched. This ensured a high degree of repeatability in the experiment, thereby maximizing its reliability.

Each specimen was positioned on the supporting anvil of the Charpy impact testing machine. The specimen was positioned in a manner that ensured precise alignment, with the standardized V-notch positioned at the midpoint of the supporting spans, oriented directly away from the edge of the pendulum's striking surface. This is to ensure that the specimen undergoes a traditional Mode I bending fracture.

3.2.5 Data post-Processing and Analysis

The first step of data processing consisted of importing the experimental data (exported as .xlsx files from the data acquisition system) into MATLAB for advanced digital signal processing. To ensure high accuracy in the results, the curve of mechanical stress was used as the main reference to determine the exact millisecond window of the pendulum's impact.

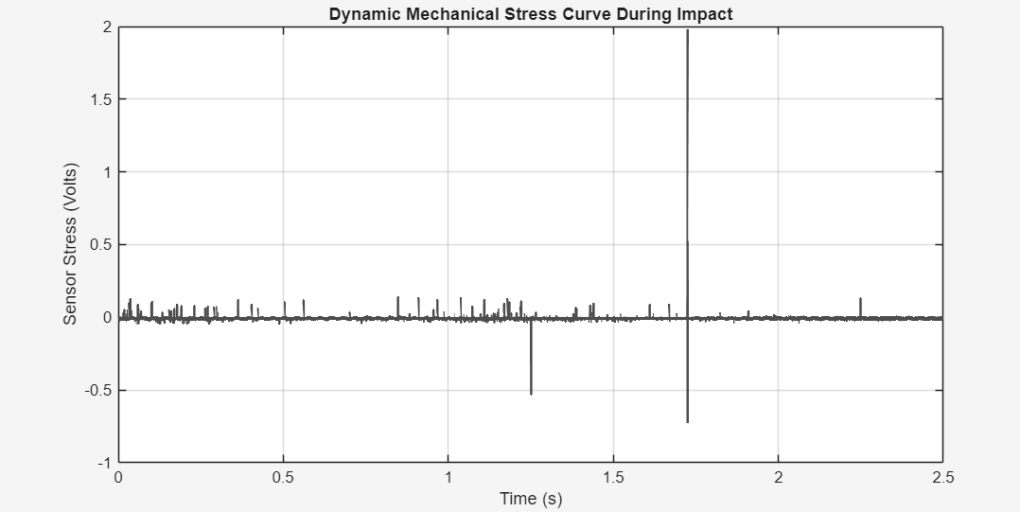

Figure 3.14 Mechanical Stress curve

The code of the Stress Curve Identification script:

```
filename = 'C:\Users\User\Downloads\Experiments Charpy\3.9.xlsx';
data = readtable(filename);

time = data.Var1;
stress = data.Var8;

figure('Name', 'Mechanical Stress Curve', 'Position', [150, 150, 900, 450]);
plot(time, stress, 'Color', [0.3 0.3 0.3], 'LineWidth', 1.5);
xlabel('Time (s)');
ylabel('Sensor Stress (Volts)');
title('Dynamic Mechanical Stress Curve During Impact');
grid on;

datacursormode on;
disp('Plot generated! Click on the start and end of the "hump" to find their exact time coordinates.');
```

Figure 3.15 Stress script

This enabled precise time-cropping of both the Acoustic Emission (AE) and Barkhausen Noise (BHN) signals. The background laboratory noise recorded before and after the fracture event was thus eliminated.

```
clear; clc; close all;

filename = 'C:\Users\User\Downloads\Experiments Charpy\3.6.xlsx';
data = readtable(filename);
time = data.Var1;
AE   = data.Var2;
BHN  = data.Var5;

t_start = 1.3;
t_end   = 1.8;
t_startAE = 1.4;
t_endAE   = 1.9;

impact_window = (time >= t_start) & (time <= t_end);
time_crop = time(impact_window);
impact_window1 = (time >= t_startAE) & (time <= t_endAE);
AE_crop   = AE(impact_window1);
BHN_crop  = BHN(impact_window);

dt = mean(diff(time_crop));
Fs = 1 / dt;
L = length(AE_crop);
Y = fft(AE_crop);
f = (0:L-1)*(Fs/L);
cutoff = 1000;
Y_clean = Y;
Y_clean(f < cutoff) = 0;
Y_clean(f > (Fs - cutoff)) = 0;
AE_clean = real(ifft(Y_clean));

```

Figure 3.16 AE and BHN signal extraction

In the preliminary analysis of the signal in the frequency domain, elevated levels of 50 Hz electromagnetic interference and their harmonics were detected in the Acoustic Emission signal. The signal domain changed into the frequency domain using the Fast Fourier Transform (FFT). The lower frequencies below 1000 Hz were mathematically filtered to zero. The signal was then transformed back into the time domain to obtain the zero-baseline Acoustic Emission signal representing the high-frequency elastic waves of material fracture.

```
[r, lags] = xcorr(AE_env_norm, BHN_env_norm, 'coeff');
[max_r, idx] = max(r);
best_lag = lags(idx);

Energy_AE  = trapz(time_crop, AE_env) * 1000000;
Energy_BHN = trapz(time_crop, BHN_env) * 1000;
Peak_AE = max(abs(AE_clean));
p = abs(AE_clean) / sum(abs(AE_clean));
p(p == 0) = [];
Entropy_AE = -sum(p .* log2(p));

fprintf('\n--- RESULTS FOR: %s ---\n', filename);
fprintf('Cross-Correlation (R): \t %.3f \n', max_r);
fprintf('Time Shift (Lags): \t %d \n', best_lag);
fprintf('Energy AE (MARSE): \t %.2f (µV*s) \n', Energy_AE);
fprintf('Energy BHN: \t\t %.2f (mV*s) \n', Energy_BHN);
fprintf('Peak AE: \t\t %.4f V \n', Peak_AE);
fprintf('Entropy AE (Shannon): \t %.4f Bits \n\n', Entropy_AE);

figure('Name', 'Final Impact Analysis', 'Position', [100, 50, 900, 600]);
subplot(3, 1, 1);
plot(time_crop, AE_crop, 'Color', [0.7 0.7 0.7]); hold on;
plot(time_crop, AE_clean, 'b', 'LineWidth', 1);
title('Raw AE (Gray) vs Clean High-Frequency AE > 1000 Hz (Blue)');
ylabel('Voltage (V)');
grid on;
subplot(3, 1, 2);
plot(time_crop, BHN_crop, 'r');
title('Raw BHN Signal');
ylabel('Voltage (V)');
grid on;
subplot(3, 1, 3);
plot(lags, r, 'k', 'LineWidth', 1.2); hold on;
plot(best_lag, max_r, 'ro', 'MarkerSize', 8, 'LineWidth', 2);
title(sprintf('Cross-Correlation (Max R = %.3f)', max_r));
xlabel('Lags');
```

Figure 3.17 Signal Computation

Following the filtration of the signal to remove noise, signal envelopes were obtained through the application of the moving average smoothing method. To synchronize the magnetic and acoustic responses and to compensate for hardware synchronization delay, the normalized cross-correlation function was applied to the Acoustic Emission and Barkhausen Noise signal envelopes. To further investigate the data usage of non-parametric indicators, entropy of the signal was introduced [25]. The main advantage of this parameter is that it is independent from threshold value, hence allowing it to be used in noisy, industrial environments. The usage of this approach is further researched. It was tested in the conducted study as an alternative perspective to Acoustic Signal counts. The entropy value was calculated using Shannon's entropy formula:

$$H = -\sum p(x) \log p(x) \quad (4)$$

Where:

- **H** represents the Shannon Entropy, which quantifies the overall complexity, uncertainty, and information content of the acoustic emission signal.
- $\boldsymbol{x}$ r epresents a distinct discrete state or amplitude bin within the analyzed acoustic signal.

- $p(x)$ is the probability of the acoustic signal occupying that specific state or amplitude bin x
- $\sum$ denotes the summation over all possible states x within the signal's distribution.
- $\log x$i is the logarithm of the probability (typically calculated in base 2, which expresses the entropy in units of 'bits').

3.2.6 Signal Analysis

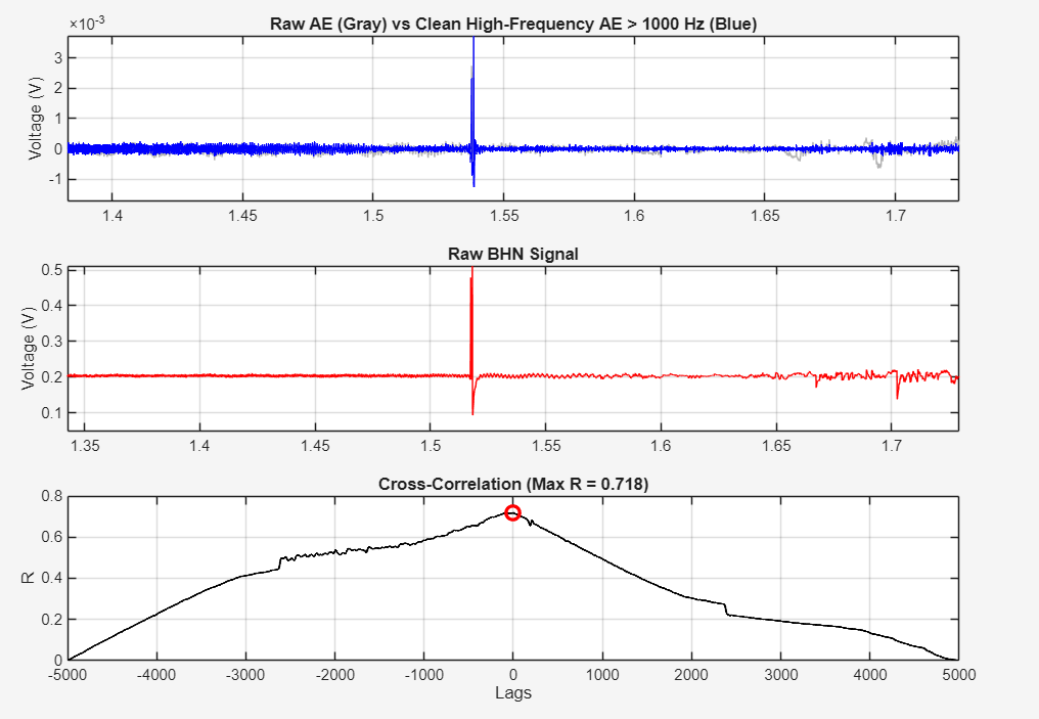

Figure 3.18 AE and BHN signal plots

To further demonstrate the effectiveness of the digital signal processing pipeline, Figure displays a sample case of the fully processed Acoustic Emission (AE) and Barkhausen Noise (BHN) signals obtained from a single Charpy impact test. The graphical representation is a validation of the applied methodology.

High-Frequency AE Isolation (Top Plot): The raw AE signal is plotted along with the FFT-filtered signal. The application of a high-pass 1000 Hz FFT filter removes unwanted baseline electromagnetic noise, thus isolating the high-frequency acoustic burst precisely coinciding with material fracture.

Magnetic Response (Middle Plot): The raw BHN signal displays a characteristic high voltage spike, coinciding with abrupt movement of magnetic domain walls in response to substantial stress applied to the material by the pendulum impact.

Signal Synchronization (Bottom Plot): The cross-correlation between normalized envelopes of AE and BHN signals reveals a high maximum correlation coefficient value (e.g., R = 0.718), thus validating signal synchronization and compensating for potential microsecond delays in the data acquisition system.

3.3 Finite Element Simulation of the Charpy Impact Test

To validate the fracture behavior from a theoretical point of view, the stress distribution during high-strain-rate deformation can be analyzed by carrying out a finite element analysis of the Charpy impact test. The impact test can be simulated by varying temperature profiles, thus comparing the results of actual experimental data.

3.3.1 3D Modeling and Geometry Preparation

The three-dimensional geometry of the Charpy impact test rig was created using initial design specifications in the SolidWorks CAD design package. The created assembly consists of the standard V-notched sample, which matches the experimental dimensions, the rigid support anvils, and the pendulum striker. The creation of geometry in a CAD environment ensures that the design meets standard test tolerances prior to importing it into the simulation environment.

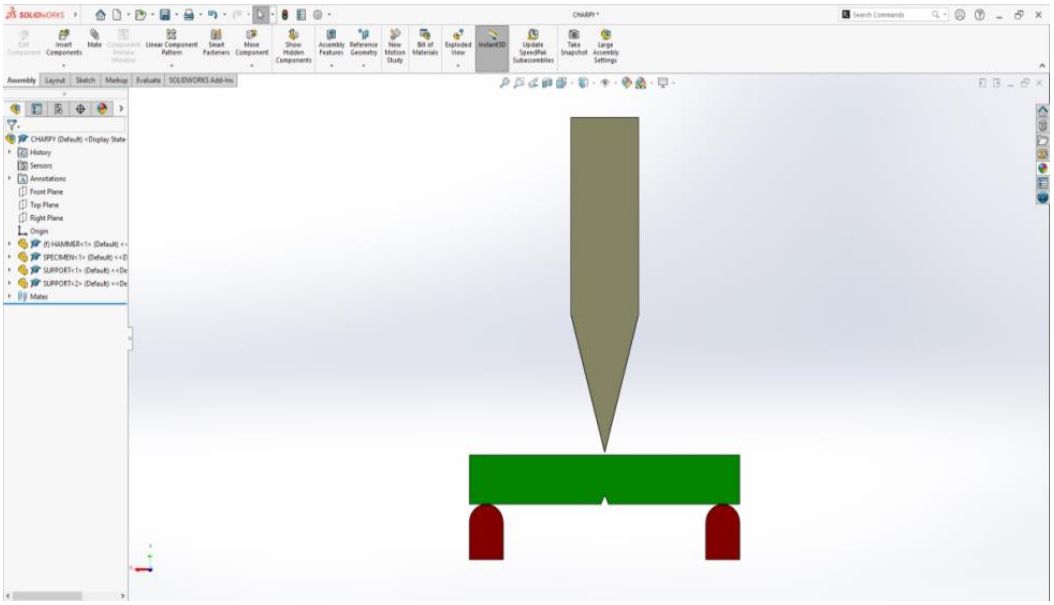

Figure 3.19 SolidWorks Assembly model

3.3.2 Explicit Dynamics Setup and Boundary Conditions

The SolidWorks assembly was imported into the ANSYS Workbench environment, and the Explicit Dynamics module was used for simulation. The module is mathematically optimized for the calculation of highly non-linear high-speed and high-strain-rate impact problems; thus, it is a default choice for performing Charpy simulations.

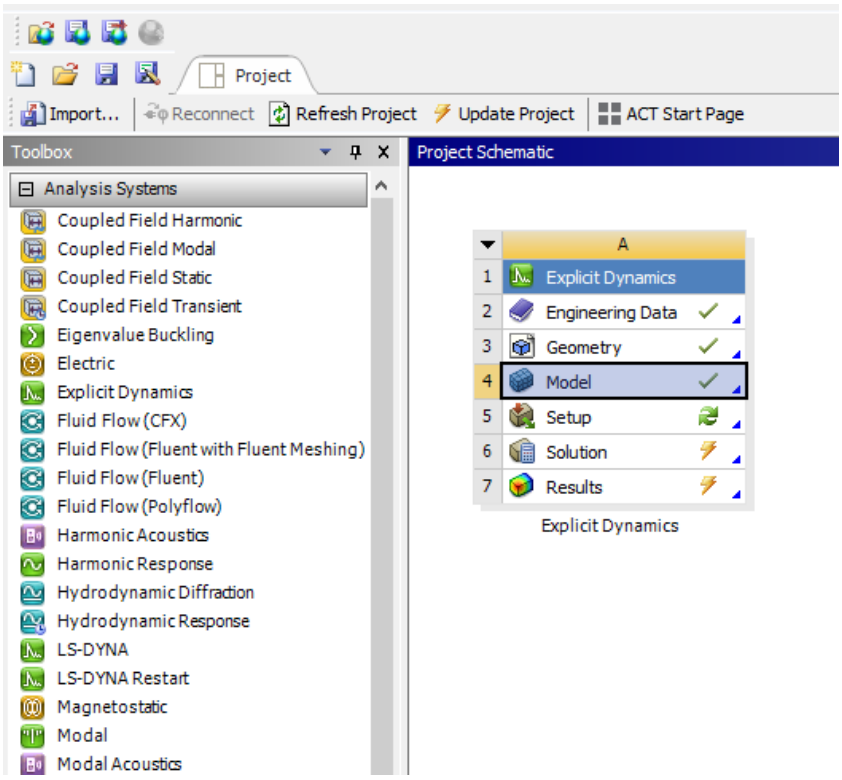

Figure 3.20 Model Tree

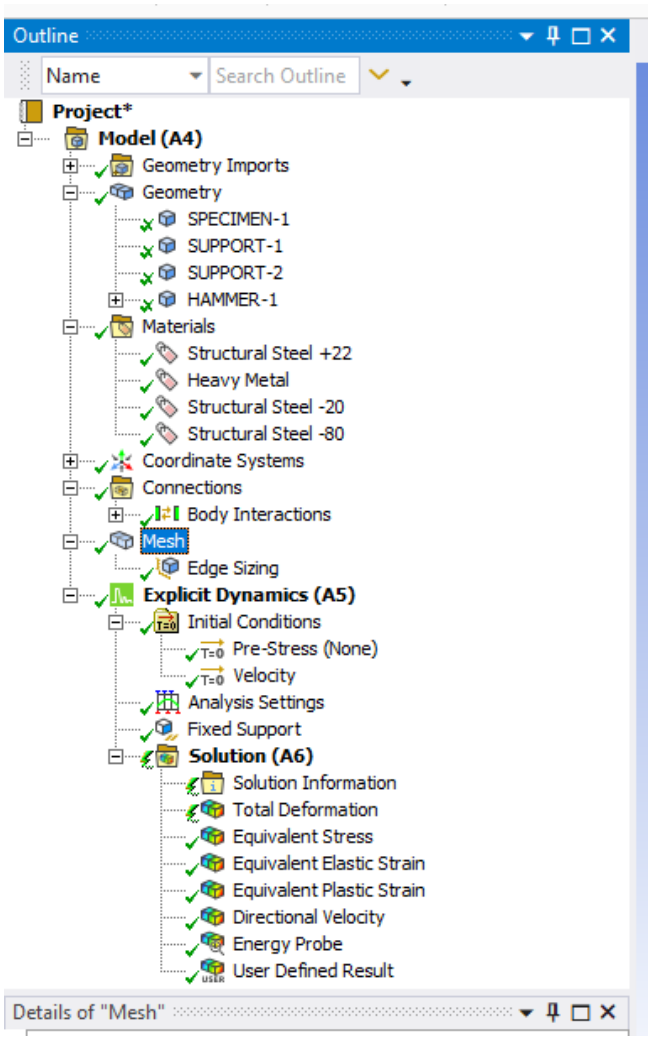

Figure 3.21 Boundary Conditions and Parameters

In the project tree of the ANSYS environment, the rigid boundary conditions were applied to the anvils to simulate the fixed support, and the pendulum striker was given an initial velocity of 5.5 m/s to correspond to the release height of the physical pendulum. Contact interactions were also applied to model the intricate contact mechanics between the striker, the deforming specimen, and the supports during the microsecond-scale window.

3.3.3 Temperature-Dependent Material Modeling

The primary computational concern is the accurate modeling of ductile-brittle transition of the material at low temperatures. Through empirical testing, the temperature significantly reduces the ductility of the material by limiting its capacity for plastic deformation.

In the ANSYS environment, a Bilinear Isotropic Hardening material model is used to simulate the behavior of the steel material. The mechanical properties of steel are altered for three different temperature environments. The Elastic Modulus remains stable across the different conditions, while the Yield Strength and Tangent Modulus are altered for each temperature profile to simulate the

increased stiffness and yield point of steel that is subjected to low-temperature working conditions.

To precisely simulate failure of the material, the mesh size was set to 1mm and 0.25mm at the V-notch of the specimen.

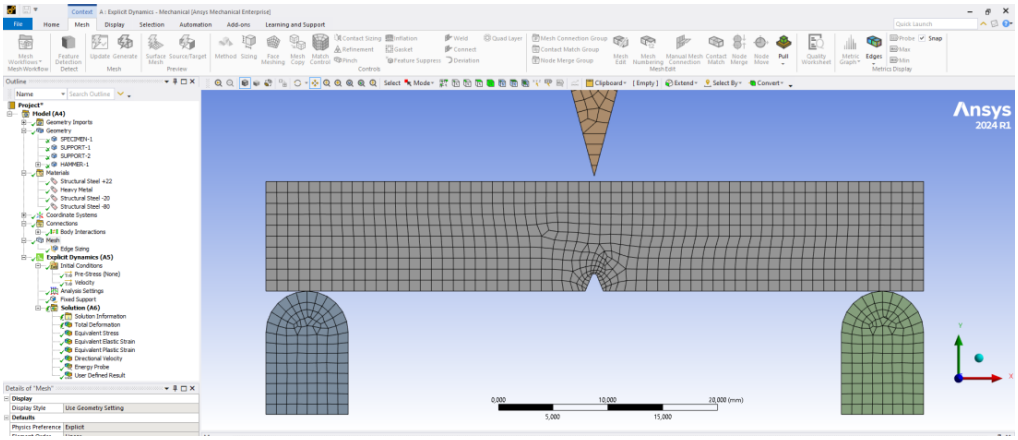

Figure 3.22 Meshing of the Specimen

Furthermore, to accurately simulate the fracture and deletion of the elements in the ANSYS environment, the Equivalent Plastic Strain at Failure is set as the primary fracture criterion for the steel material. The value is significantly reduced for the low-temperature profiles to simulate the loss of ductility in steel:

- Profile 1 (Room Temperature, 22°C): Plastic strain at failure is set to 0.35. The high value of equivalent plastic strain allows for significant distortion and energy absorption before deletion of the element, thereby simulating a ductile fracture due to bending forces.

- Profile 2 (Sub-zero, -20°C): Plastic strain at failure is reduced to 0.18. The value is significantly reduced to simulate a transitional phase of yielding before fracture occurs.

- Profile 3 (Deep Freeze, -80°C): Plastic strain at failure is limited to 0.05. The low value of equivalent plastic strain forces an immediate fracture upon yielding of the steel material, thereby simulating a low-energy fracture due to cleavage forces.

Through these different failure criteria for each temperature profile, the ANSYS solver can accurately simulate the macroscopic transition from ductile to brittle fracture.

3.3.4 Meshing adjustment

At first, the global mesh generation was based on 2 mm elements without any local refinement near the V-notch. The rough mesh helped to quickly perform impact simulations and test the proper implementation of global geometry, rigid bodies' behavior, material properties, and boundary conditions.

Afterwards, it became evident that a 2 mm mesh was not enough to correctly calculate the extreme stress concentration and plastic strain gradients near the V-notch tip during the high-velocity collision of the plates.

In fracture mechanics and explicit dynamics, the precision of simulations using the equivalent plastic strain at failure-based element-deletion technique depends on the mesh density near the crack initiation point. A coarse mesh causes averaging the maximum stresses over a broader volume, resulting in the incorrect modeling of the ductile-to-brittle transition and energy dissipation.

To compensate for this issue, a mesh refinement technique was applied. Firstly, the element size in the global mesh of the specimen was decreased from 2 to 1 mm to correctly estimate bending deformation of the body. Secondly, the faces of the V-notch received specific sizing controls with elements of 0.25 mm size.

With such refinement, there will be enough integration points in the curved region of the V-notch for calculating the extremely high stress distribution before breaking. Despite the significant increase in the number of nodes and elements leading to an increased solving time of the problem in the ANSYS Explicit Dynamics module, this modification was required to provide a reliable and detailed analysis of crack initiation and element deletion at different temperatures.

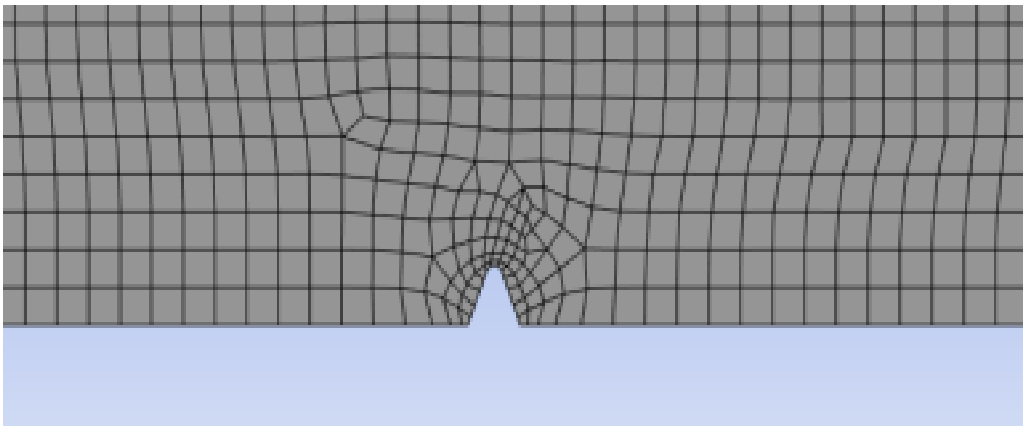

Figure 3.23 Refined mesh

4 Results

4.1 Summary of Extracted NDT Parameters

After digital signal processing and using the high-pass noise filtration based on the Fast Fourier Transform with a cutoff at 1,000 Hz, as described in Chapter 3, the following quantitative parameters were extracted for a short window of 10 ms for each sample: Peak Acoustic Emission (AE), Peak Barkhausen Noise (BHN), Acoustic Energy (MARSE), Barkhausen Noise Energy, Shannon Entropy, and the maximum Cross-Correlation coefficients.

Table 4.1 Signal Parameters

Specimen	Cooling Method	Impact Energy (J)	Peak AE (V)	Peak BHN (V	Energy AE	Energy BHN	Shannon Entrop	Primary Cros	Secondary Corr (E
2.2	Air	77.84	0.0019	0.0358	0.81	0.03	5.1567	-0.61	0.79
3.2	Water	57.32	0.0028	0.581	1.21	0.2	5.0426	0.891	0.855
3.3	Water	45.54	0.0009	0.0718	0.78	0.04	5.573	0.681	0.795
3.4	Water	78.94	0.0017	0.0577	0.98	0.04	5.3074	0.743	0.613
3.5	Water	79.86	0.0015	0.0898	0.74	0.04	5.4418	0.902	0.882
3.6	Water	81.48	0.0046	0.3753	2.06	0.16	4.91	0.988	0.906
3.7	Water	61.49	0.0033	0.1611	1.86	0.11	5.2166	0.61	0.583
3.8	Water	63.34	0.0007	0.1593	0.6	0.07	5.4543	0.641	0.608
3.9	Water	31.73	0.0019	0.17	1.41	0.08	5.4391	0.506	0.582

4.1.1 Cross-Correlation analysis

To guarantee that the experimental configuration was able to correctly capture the simultaneous physical phenomena that accompany fracture processes, a dual-layer cross-correlation analysis was carried out. The principal normalized cross-correlation between the AE and Barkhausen-Noise (BHN) envelopes revealed highly significant coefficients, with values up to $|R| = 0.988$ recorded for specimen 3.6. This suggests a strict synchronization between the acoustic shockwave resulting from crack propagation and changes in magnetic domains. Furthermore, a second-order correlation analysis was also carried out by cross-correlating the normalized BHN signal with the primary correlation curve.

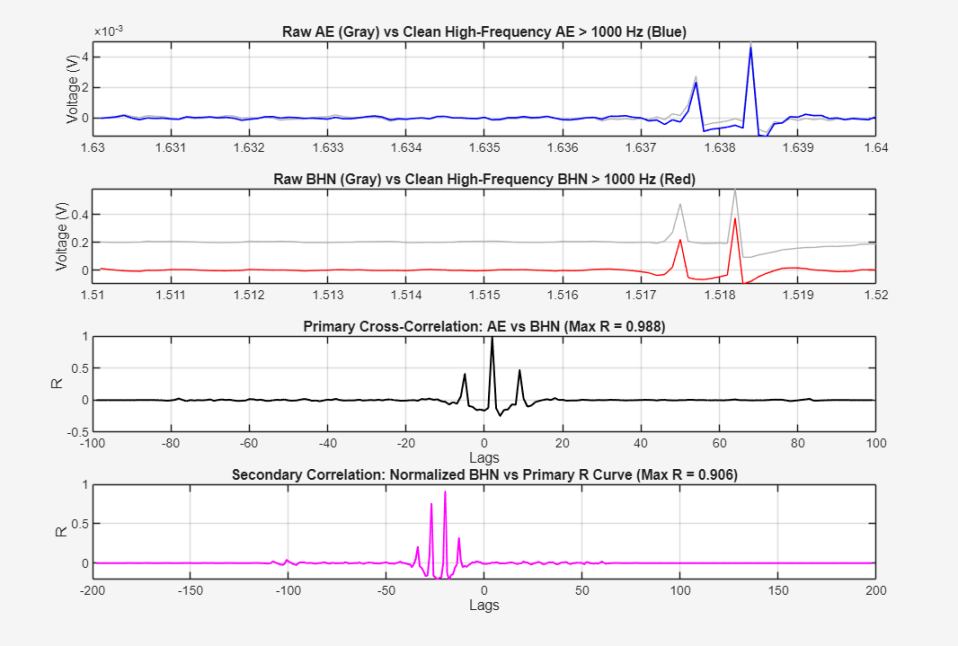

Figure 4.1 AE and BHN signal parameters 3.6

The high values obtained in this case (e.g., R = 0.906 recorded for specimen 3.6) confirm that this degree of time-synchronization is not a result of a random statistical occurrence but rather that the periodicity in localized magnetic domain jumps is a direct mirror-image of the envelope of the dynamic acoustic wave.

Another example of this phenomenon is sample 3.2:

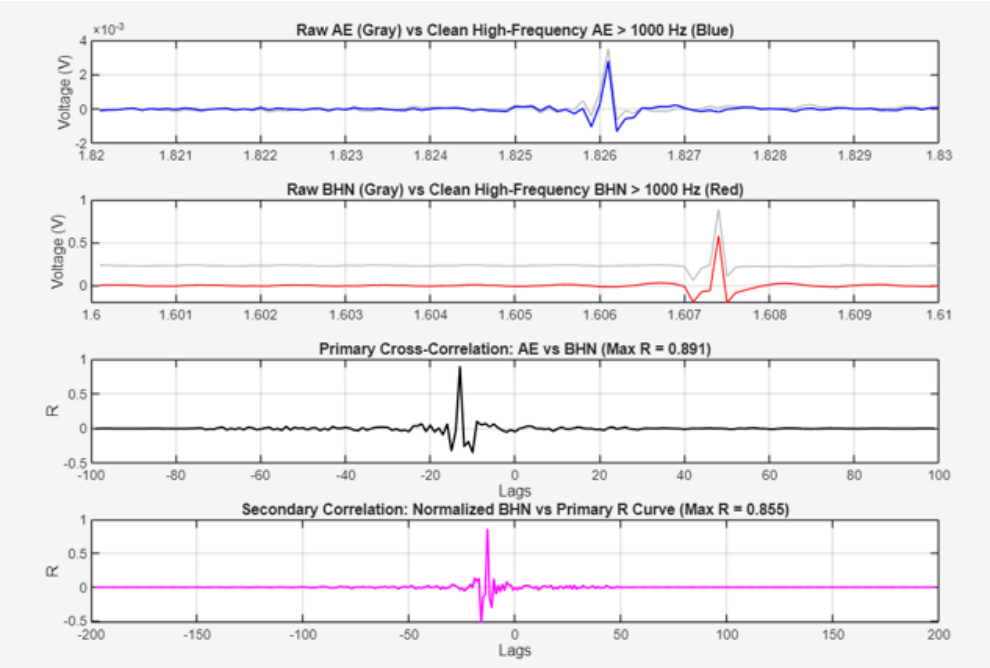

Figure 4.2 AE and BHN Parameters 3.2

4.1.2 Villari Effect Observation

By recording the Barkhausen Noise simultaneously during the Charpy impact, this study successfully captured the dynamic magneto-elastic response, also referred to as the Villari effect. The linear regression analysis of Peak Acoustic Emission (AE) vs. Peak Barkhausen Noise (BHN) shows a strong positive correlation.

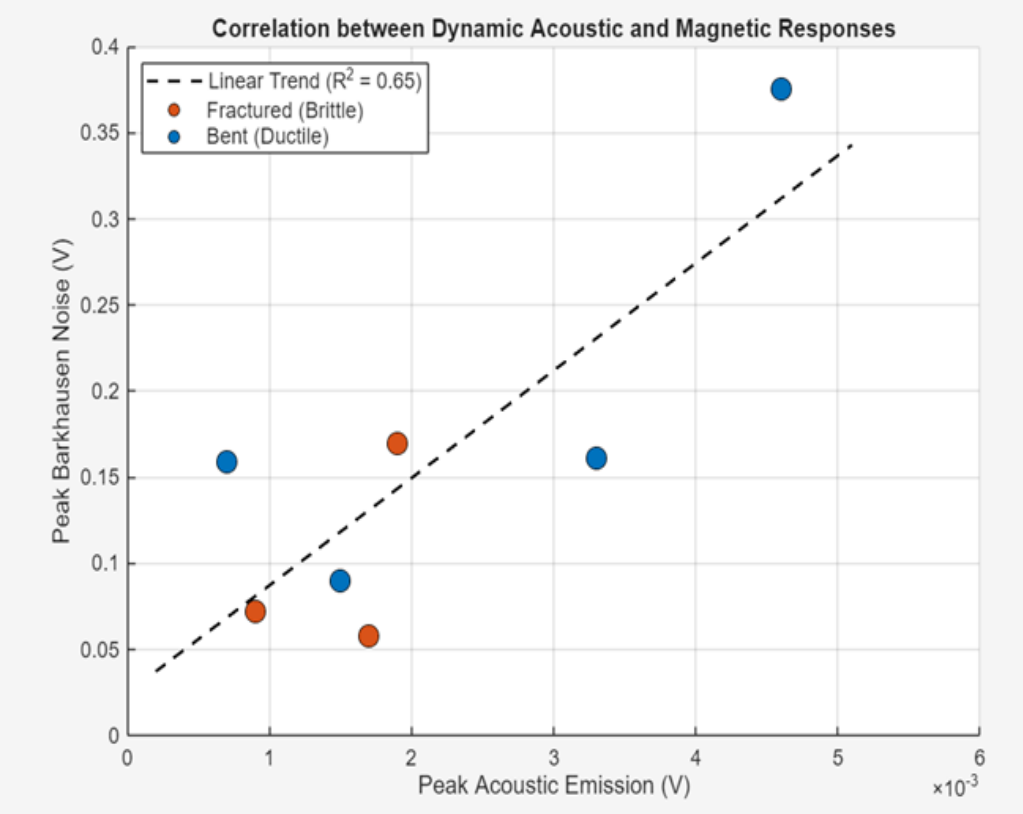

Figure 4.3 Correlation between AE and BHN peaks

This result suggests that the peak of the acoustic emission can be a reliable predictor of the dynamic magnetic stress response.

Dynamic magnetic response behavior in instrumented impact testing is based on the basic theory of magnetoelasticity, where the Villari effect determines the dependence of the state of magnetization on the applied stresses. In ferromagnetic materials, the Villari effect defines the phenomenon that the magnetization state of a material is affected by mechanical stress, which results in a change in magnetic anisotropy energy.

Magnetic domains represent regions of magnetization that occur in ferromagnets. Each magnetic domain is characterized by saturation magnetization and separated from other domains by domain walls. Positive magnetostrictive materials have their magnetic domains biased in energy because of external mechanical stress. When tensile stress is applied, the energy associated with magnetoelasticity to orient magnetic domains parallel to the direction of the applied stress decreases, while compressive stress induces perpendicular alignment of the domains, hence preventing parallel magnetization.

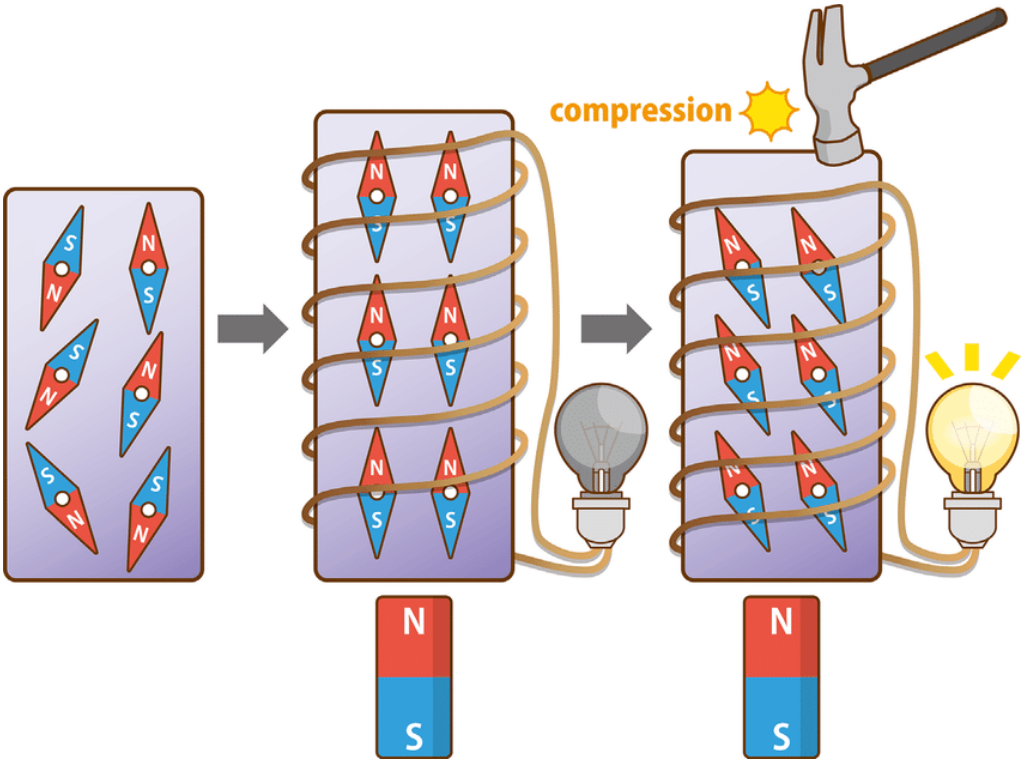

Figure 4.4 Magnetization direction in the metal [26]

It is shown in figure 4.4 that the material with no internal state does not have a uniform orientation of a magnetic field. However, after the mechanical stress was applied, the orientation of a magnetic field tilted slightly.

4.1.3 Fracture Mode Classification

The extracted NDT parameters successfully differentiated the fracture mechanics of the specimens, aligning perfectly with macroscopic visual observations of the post-impact samples (broken vs. bent).

- Ductile Bending (High Energy): Specimens that absorbed the highest impact of energy (e.g., Specimen 3.6 at 81.48 J) exhibited macroscopic bending and severe plastic deformation. These specimens had the highest level of peak amplitude for both signals, with the highest peak amplitude for the acoustic emissions (Peak AE = 0.0046 V) and the highest peak amplitude for the magnetic stress (Peak BHN = 0.3753 V), indicative of the sudden release of large amounts of stored elastic strain energy.

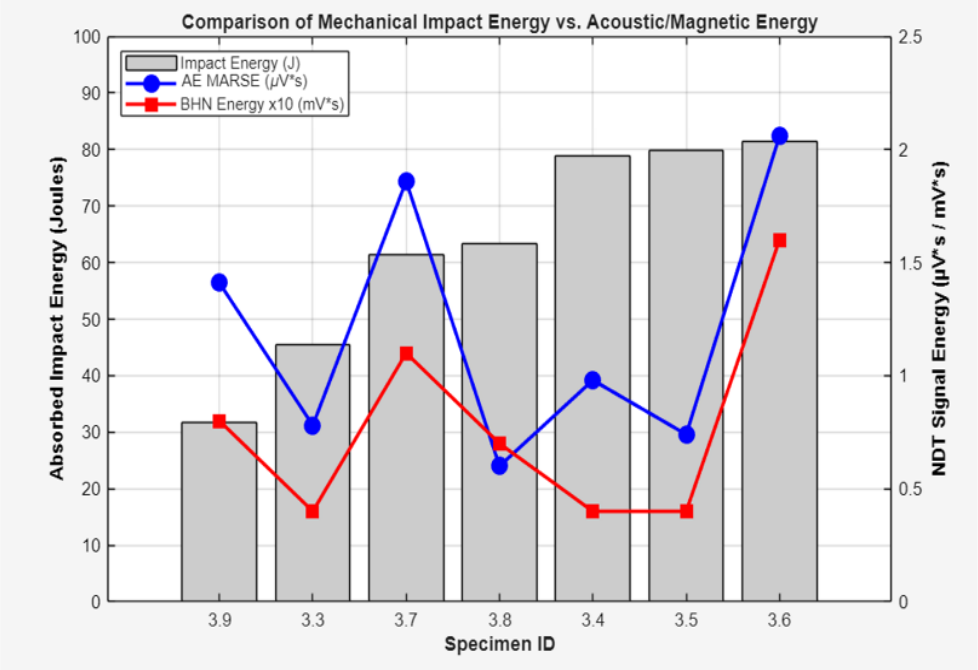

Figure 4.5 MARSE Energy and Impact Energy Correlation

- Brittle Fracture (Low Energy): The specimens that had an abrupt brittle fragmentation (e.g., Specimen 3.9, 31.73 J; Specimen 3.3, 45.54 J) had significantly lower peak amplitudes for both sensors. The rapid micro-cleavage fragmentation did not have sufficient time to generate significant magneto-elastic stress waves.

Figure 4.6 Sample 3.1 after the Impact

As can be seen in the image, the specimen 3.1 breaks into two parts, which the brittle nature of the deformation in the material.

Figure 4.7 Specimen 3.6 after the Impact

However, as Figure 4.6 depicts the specimen, 3.6 underwent a Plastic deformation.

4.1.4 The Shannon Entropy Analysis

Regression analysis of the water-cooled specimens showed an unexpected inverse relationship between the absorbed impact energy and the Shannon entropy of the acoustic emission (AE) signals.

While conventional signal processing principles relate high-energy events to complex signal behavior, the experimental data show an opposite relationship. The most ductile specimen (3.6), which absorbed the maximum energy (81.48 J), showed the lowest acoustic entropy (4.91 Bits), whereas the low energy absorption of the brittle specimens (e.g., specimen 3.3 and 45.54 J) showed high entropy values (> 5.5 Bits).

From a fracture mechanics viewpoint, these data indicate that high-energy ductile fracture is a relatively ordered process. The elevated levels of localized plastic deformation cause a high concentration of acoustic energy release, which corresponds to low mathematical chaos. In contrast, low-energy brittle fracture involves a high rate of microscopic cleavage and crack branching, causing a chaotic and long-lasting acoustic emission signal, which is indicated by high signal entropy.

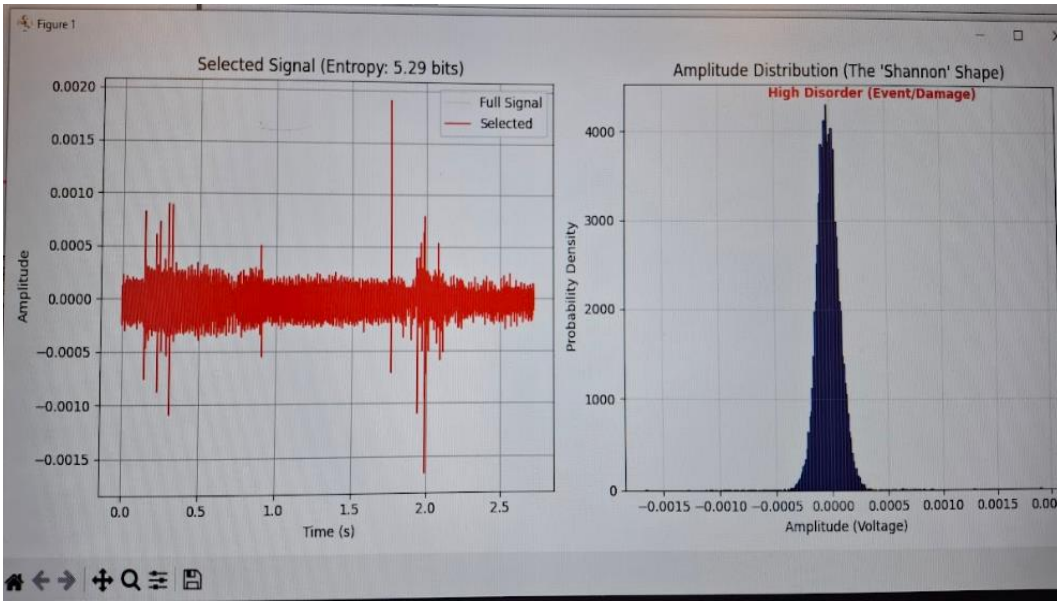

Figure 4.8 Signal Entropy measurement

4.2 Explicit Dynamics Simulation Result

Through adjustments in Equivalent Plastic Strain at Failure under three separate temperature conditions, the simulation mirrored the large-scale shift from ductile to brittle behavior. Validation of the physical Charpy test outcomes emerged via assessment of data from ANSYS Explicit Dynamics finite element modeling.

1.**Room temperature (22°C)** - the material showed notable ductility during bending tests. When struck by the pendulum, the area near the V-notch deformed heavily but did not fracture immediately. Such response mirrors what was seen in certain physical samples, like Specimen 3.6, which exhibited extreme flexibility under impact. High readings in both dynamic Barkhausen Noise and Acoustic Emission were recorded, confirming sustained deformation activity before eventual failure.

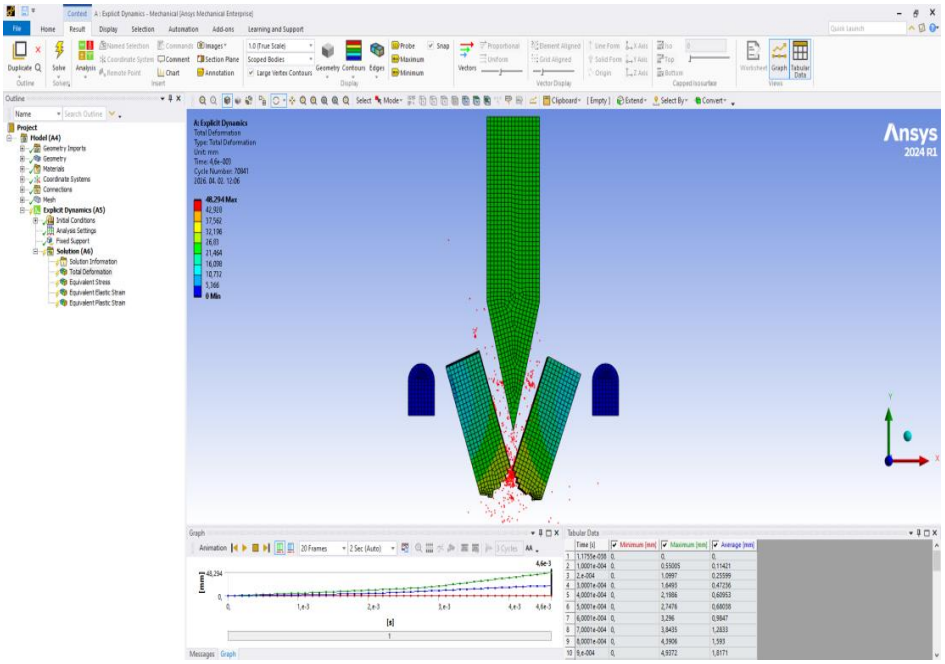

Figure 4.9 Room temperature simulation

2. **-20°C Temperature** - the model showed a shift toward transitional cracking. The plastic strain limit was reduced to 0.18. Cracking began after some yielding appeared near the notch base. A small bend formed there, visible on a large scale. Fracture moved quickly once initiated. Energy absorption was limited but still present before breakage occurred. This indicates a mixed-mode fracture, representing the threshold region of the ductile-to-brittle transition curve.

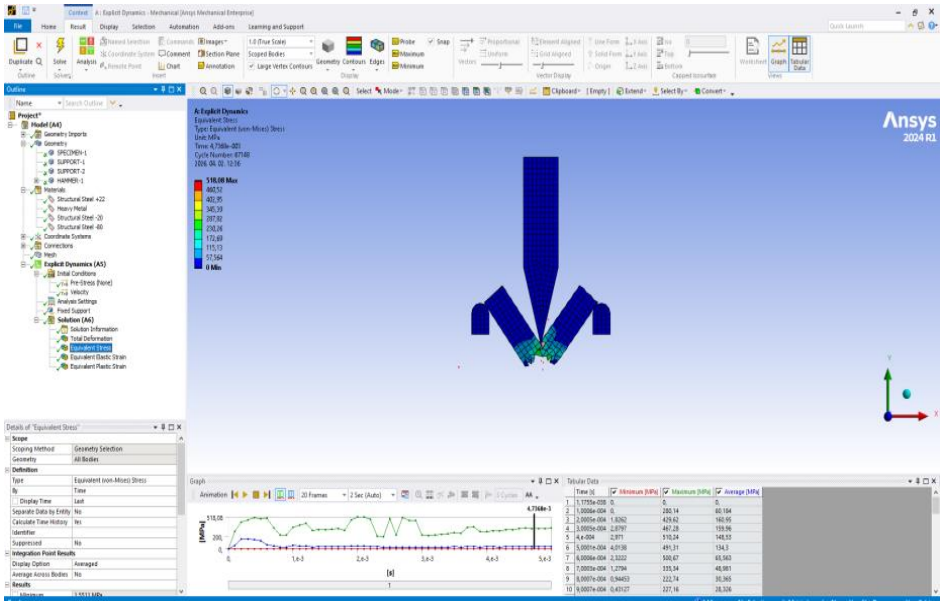

Figure 4.10 -20°C Simulation

3. -80°C Temperature - With plastic strain capped at just 0.05, failure struck fast when force applied. Instead of bending first, elements vanished right after contact. Cracks occurred along high-stress zones with little warning deformation. Simulation patterns matched fragile test samples like 3.3 and 3.9. Sharp breaks led to faint magnetic pulses alongside noisy, disordered sound waves.

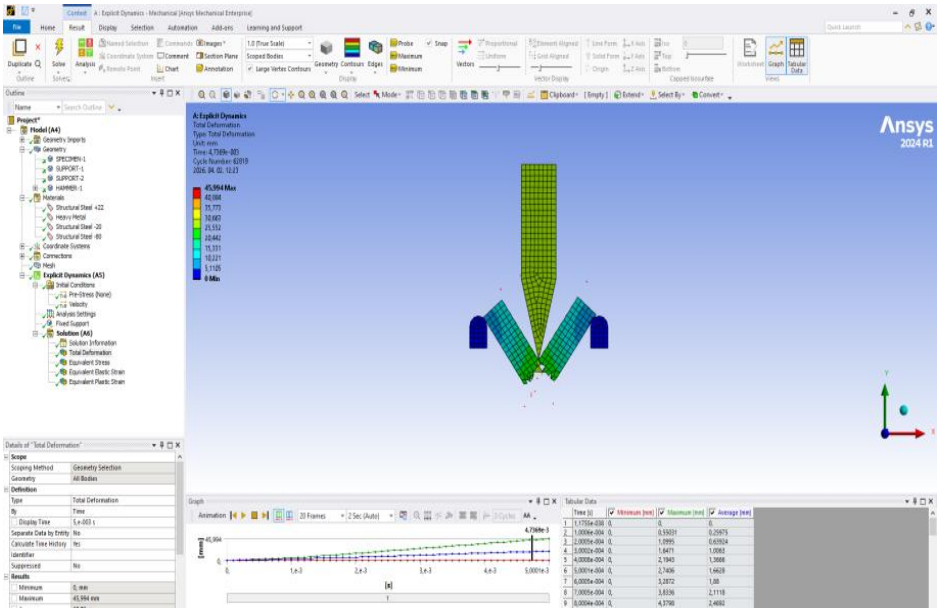

Figure 4.11 -80°C Simulation

Despite differing methods, results aligned closely between simulation and experiment. Simulations reflected what sensors recorded physically. Threshold shifts in strain behavior explained signal variations observed earlier. Simulated stress waves resembled those detected without needing calibration tricks. This numerical consistency supports the idea that material degradation alters wave propagation. Observations from lab tests found a parallel in digital environments through parameter tuning.

5 Conclusions

This work introduces a new combination of non-destructive testing methods, using high-frequency acoustic emissions alongside dynamic Barkhausen noise, tested under controlled impact conditions. Through structured experiments, signals were captured and examined with algorithmic tools, supporting each key outcome. Findings confirm that the approach works effectively, meeting the central goals set at the start. Rather than relying on conventional measures, real-time responses from both techniques provided complementary insights into material behavior. Each phase of analysis contributed distinct evidence, reinforcing the reliability of results. The method proves feasible, grounded in measurable data rather than assumptions

5.1 Design of a Synchronized AE-BHN Experimental Setup

A series of tests captured fast acoustic and magnetic signals during sudden impacts, using a setup built specifically for microsecond-level precision. Triggered by an optical sensor, a custom-built recording system in LabVIEW logged multiple data channels steadily, avoiding delays. With processing power focused on clarity, FFT-based filters removed low-frequency noise above 1000 Hz, clearing the path for clean detection. Clear patterns emerged only after background noise was removed, revealing sharp waveforms tied to cracking events.

5.2 Correlation of AE and BHN Signal with Residual stress

Analyzing the AE signal characteristics yielded a strong correlation between the thermal treatment specimens underwent and intensity of the BHN signal. With normalized cross-correlation, timing alignment between sound pulses and shifts in magnetic regions became clear - mathematical results reached |R| values as high as 0.988. Notably, the inverse relationship between Shannon Entropy and the absorbed impact of energy was detected. It was concluded that high energy, ductile tearing is a more „organized” process than brittle shattering. These synchronized signals successfully detect the pre-existing residual stress profiles left by prior thermal treatments, fulfilling the primary objective of this research.

5.3 Method for Evaluating Residual Stress

This study introduced a new diagnostic method for evaluating internal stress states through capturing changes in magnetic behavior when materials are under strain - the Villari effect. During impact events, data from acoustic signals and magnetic noise were gathered at once; analysis revealed a strong linear regression between them. It turned out that Peak Acoustic Emission amplitude released matched

closely with the Peak Barkhausen Noise spike. This method successfully differentiated between the highly stressed microstructures of water-quenched steel and the relaxed, low-stress states of air-cooled steel based solely on their dynamic magnetic responses.

5.4 Comparison with Existing Material Stress Analysis Methods

In comparison with the traditional methods for measuring residual stress, including X-ray diffraction (XRD) and hole-drilling technique, the AE-BHN methodology demonstrates several distinct diagnostic benefits. While the hole-drilling technique can provide reliable results in terms of strain measurement, it is semi-destructive, meaning that it causes permanent changes within the material by creating another stress concentration point. The AE-BHN technology, on the other hand, is completely non-invasive, allowing the structure of the part under consideration to remain intact. Another significant difference between XRD and the current method lies in the fact that while the former can be considered a static approach and be applied exclusively to stationary parts, the latter can be described as dynamic because it captures events happening in real time.

5.5 Final Summary

The combination of Acoustic Emission and Barkhausen Noise testing provides a comprehensive approach to the evaluation of the structural condition and analysis of residual stresses in a non-destructive manner. The approach presented within this thesis forms the basis for further research in structural health monitoring systems. Based on the results obtained from this study, it can be noted that using the combination of High Frequency Acoustic Emission (AE) and Barkhausen Noise (BN) Analysis successfully creates a bridge between real-time fracture detection and post-fracture evaluation of the material's stress state. Contrary to conventional approaches, such as hole drilling, which are destructive, causing additional stress concentration, the AE-BN method remains fully non-destructive, hence maintaining the integrity of the material under study. Furthermore, the inverse correlation between Shannon entropy and energy absorbed opens a new opportunity for developing a non-parametric measure to differentiate between ductile and brittle fracture behavior in ferromagnetic materials.

List of references/Bibliography

[1] Diegel, O. – Wohlers, T.: How residual stress can cause major build failures, and what you can do to prevent it, In: Metal AM {online}, https://www.metal-am.com/articles/how-residual-stress-can-cause-major-build-failures-in-3d-printing/ (Accessed: 17.04.2026 11:30 a.m.)
[2] Guo, J. – Fu, H. – Pan, B. – Kang, R.: Recent progress of residual stress measurement methods: A review, In: Chinese Journal of Aeronautics, 2021, 34(1), p. 54–78. DOI: 10.1016/j.cja.2019.10.010
[3] Piotrowski, L. – Chmielewski, M.: Self-Calibrating Stress Measurement System Based on Multidirectional Barkhausen Noise Measurements. In: Journal of Non-destructive Evaluation, 2024. 43/119. https://doi.org/10.1007/s10921-024-01137-x
[4] SinTTechnology Ltd.: Residual Stress Measurement. In: SinTTechnology {online} https://www.sintechnology.com/portfolio-articoli/residual-stress-measurement/ (Accessed: 14.04.2025)
[5] Anton Paar: X-ray Diffraction (XRD). In: Anton Paar Wiki {online} https://wiki.anton-paar.com/hu-hu/x-ray-diffraction-xrd/ (Accessed: 12.05.2025 12:23 p.m.)
[6] Deveci, M.: Stresstech Bulletin 12: Measurement Methods of Residual Stresses, In: Stresstech Articles {online} https://www.stresstech.com/stresstech-bulletin-12-measurement-methods-of-residual-stresses/ (Accessed: 15.04.2025, 10:00 a.m.)
[7] LibreTexts Chemistry: 7.05: Neutron Diffraction. In: LibreTexts {online} https://chem.libretexts.org/Bookshelves/Analytical_Chemistry/Physical_Methods_in_Chemistry_and_Nano_Science_(Barron)/07%3A_Molecular_and_Solid_State_Structure/7.05%3A_Neutron_Diffraction (Accessed: 12.05.2025 12:23 p.m.)
[8] Sonats: Hole drilling for residual stress measurement, Hole drilling for residual stress measurements and analyses, Diagram of the principle of the incremental drilling method, In: Sonats-et {online} https://sonats-et.com/wp-content/uploads/sites/3/2019/03/Hole-drilling-method-principle.jpg (Accessed: 12.05.2025 12:23 p.m.)
[9] Takashima, Y. – Mitsuru, M.: Evaluation Method for Fracture Mechanics-Based Material Toughness from Charpy Impact Test, In: Materials Science Forum, 2006, 512, p. 61–66. ISSN: 1662-9752. DOI: 10.4028/www.scientific.net/MSF.512.61
[10] Rossoll, A: Mechanical aspects of the Charpy impact test, Nuclear Engineering and Design, Volume 188, Issue 2, 1999, Pages 217-229, ISSN 0029-5493, https://doi.org/10.1016/S0029-5493(99)00017-5.

[11] Feng, G: Effects of Temperature on the Relationship between Mode-I Fracture Toughness and Tensile Strength of Rock. Applied Sciences. 2019; 9(7):1326. https://doi.org/10.3390/app9071326
[12] AENDT: What is an acoustic emission sensor? What is the principle and types of AE sensors? In: QAWRUMS {online}, https://www.aendt.ru/uploads/allimg/221122/1-2211221455560-L.png (Accessed: 17.04.2026 11:10 a.m.)
[13] Muhammad U.: Burst-informed acoustic emission framework for explainable failure diagnosis in milling machines, Engineering Failure Analysis, Volume 185, 2026, 110373, ISSN 1350-6307, https://doi.org/10.1016/j.engfailanal.2025.110373
[14] Tiboni, G. – da Silva C.H.: Application of Acoustic Emission for Monitoring Erosive Wear Tests of Low Carbon Steel by Solid Particles. In: 2nd International Brazilian Conference on Tribology, Foz do Iguaçu, Brazil, 2014. DOI: 10.5151/1472-5836-25717
[15] Integrity Diagnostics: Introduction to Acoustic Emission. In: Integrity Diagnostics {online} https://www.idinspections.com/acoustic-emission-phenomenon/ (Accessed: 12.05.2025 12:23 p.m.)
[16] Carpinteri, A.: Influence of damage in the acoustic emission parameters, Cement and Concrete Composites, Volume 44, 2013, p. 9-16, ISSN 0958-9465, https://doi.org/10.1016/j.cemconcomp.2013.08.001.
[17] Tronskar, J. P. – Mannan, M. A. – Lai, M. O.: Application of Acoustic Emission for Measuring Crack Initiation Toughness in Instrumented Charpy Impact Testing. In: Journal of Testing and Evaluation, Vol. 31, No. 3, 2003, p. 247–258. https://doi.org/10.1520/JTE12420J
[18] Zhao, L. – Kang, L. – Yao, S.: Research and Application of Acoustic Emission Signal Processing Technology, in IEEE Access, vol. 7, pp. 984-993, 2019, DOI: 10.1109/ACCESS.2018.2886095
[19] G. Balogh, – I. Szabó: New procedure to combine cad modeling, FEM simulation and Barkhausen noise stress analysis in sheet metal forming,2012, ACTA PHYSICA DEBRECINA, XLVI, 9
[20] Sorsa, A. – Santa-aho, S. – Wartiainen,:Effect of Shot Peening Parameters to Residual Stress Profiles and Barkhausen Noise. J Nondestructive Eval 37, 10 (2018). https://doi.org/10.1007/s10921-018-0463-7
[21] Deveci, M.: What is Barkhausen Noise? In: Medium {online} https://murat-deveci.medium.com/what-is-barkhausen-noise-ea292cb9bec2 (Accessed: 12.05.2025 12:23 p.m.)
[22] Binayaka, N. : Material Characterization using Barkhausen Noise Analysis Technique - A Review, Indian Journal of Science and Technology, Vol 10(14), April 2017 DOI: 10.17485/ijst/2017/v10i14/109697. ISSN (Online): 0974-5645
[23] Stresstech: Barkhausen Noise Analysis. In: Stresstech {online} https://www.stresstech.com/technologies/non-destructive-testing-methods/barkhausen-noise-analysis/ (Accessed: 14.04.2025 10:55 a.m.)

[24] Kawata, Osamu: Two Step Ductile to Brittle Transition Behavior on Ferrite + Pearlite Structure Steel Sheet, In: ISIJ International, 2017, 57(7), p. 1282–1288. DOI: 10.2355/isijinternational.ISIJINT-2017-026
[25] Chai, M. – Zhang, Z. – Duan, Q.: A new qualitative acoustic emission parameter based on Shannon's entropy for damage monitoring, Mechanical Systems and Signal Processing, Volume 100, Pages 617-629, 2018
[26] Fumio, N. – Marina, F.: A Review on Piezoelectric, Magnetostrictive, and Magnetoelectric Materials and Device Technologies for Energy Harvesting Applications, November 2017, Advanced Engineering Materials 20(5):1700743, DOI: 10.1002/adem.201700743